2019-04-01

The Investigation of Nickel-Based Catalysts for the Oxidative Dehydrogenation of Ethane

Justin Lane Park
Brigham Young University

The Investigation of Nickel-Based Catalysts for the Oxidative Dehydrogenation of Ethane

Justin Lane Park

A dissertation submitted to the faculty of
Brigham Young University
in partial fulfillment of the requirements for the degree of

Doctor of Philosophy

Kara J. Stowers, Chair
Morris Dee Argyle
David John Michaelis
Brian F. Woodfield
Steven L. Castle

Department of Chemistry and Biochemistry

Brigham Young University

ABSTRACT

The Investigation of Nickel-Based Catalysts for the Oxidative Dehydrogenation of Ethane

Justin Lane Park
Department of Chemistry and Biochemistry, BYU
Doctor of Philosophy

The advancement of creating ethylene from ethane via oxidative dehydrogenation (ODH) rather than the traditional direct dehydrogenation is right on the cusp of commercialization. The oxidative pathway provides a novel route that reduces the operating temperature of this reaction by 400-500°C. A variety of metals including Mo, V, and Ni that have redox properties suitable for the partial oxidation of small chain alkanes have been investigated. Currently, a MoVNbTe oxide is the most promising catalyst but it suffers from a long and difficult preparation method and the combination of four expensive metals. Nickel based catalysts have also shown great promise but are limited by the reactivity of the oxygen species on the surface of the catalyst. In this manuscript, the details for improving the activity of the nickel and altering the activation mechanism are outlined.

Bulk CeNiNb oxide catalysts were shown to almost double the rate of ethylene yields at temperatures as low as 300°C. This is partially related to the improved rate of oxygen adsorption and transfer to the active oxygens on the nickel oxide via the ceria additive. However, with further characterization of these materials, it was shown that there is likely an interaction between the Ce and Nb, forming a Ce – O – Nb linkage that is also selective towards ethylene. This facilitates a higher activity of the catalyst by creating two redox active sites.

The improved rates of ethylene formation observed with these catalysts led to the initial development of a commercially viable nickel based catalyst. The support interactions of NiO with a novel silica doped alumina support show higher yields than previously reported studies of NiO on alumina for ODH. These initial metal support interactions show that the addition of the niobium and ceria to this catalyst should give ethylene yields that are satisfactory for the commercialization of this catalyst.

Keywords: catalysis, oxidative dehydrogenation, nickel, ceria, niobium, titania, alumina support

ACKNOWLEDGEMENTS

I want to thank Kara Stowers for being my mentor. She has played a key role in directing me to the right opportunities for research, funding, ultimately graduation and career opportunities.

I want to thank my parents for always believing in me and pushing me to work hard in every aspect of my life.

I want to thank all the graduate and undergraduate students that have been there as support and to exchange ideas.

I want to thank the Quarry for giving me a place to decompress and relieve stress.

TABLE OF CONTENTS

LIST OF FIGURES

LIST OF TABLES

Chapter 1: Introduction

Our planet has been experiencing a change in climate since as early as 1978.[1] As a result the atmospheric and oceanic temperatures have increased. These relative small changes in temperature (from a human perspective) have begun to impact ecosystems[2,3] and weather[4] patterns across the world. For example, the Great Barrier Reef has experienced major bleaching from increased carbon dioxide in recent years, which has been attributed to changes of only 4°C in average temperature.[5] In another study, experiments showed that over 1,000 different species of plants and animals are exhibiting small changes in their evolutionary history directly related to temperature increases.[2] One of the scariest potential results of the changes in the oceanic temperatures is that drastic changes in virus evolution and virus host interactions are predicted.[3] It is very clear from these and other studies that the slow rise in global temperatures is having an impact on our environment.

In order to halt or limit the impact of global warming, we first need to find the source of the temperature increases and then find viable solutions to combat those increases. The release of massive amount of greenhouse gases combined with deforestation is, in most cases, attributed to the observed increase in temperature over the last few decades.[6] Greenhouse gases lead to what is called the greenhouse effect. This occurs when solar radiation entering the atmosphere, reflects off of the earth's surface, and gets trapped by then reflecting off of gases in the atmosphere. With increases in population and global industrialization, more gases have been released into the atmosphere trapping solar rays longer, which has led to the increase in temperature. One way to limit the rise in global temperature is for the world to limit the amount of carbon emissions we produce.

Greenhouse gases come from a variety of sources. According to the EPA,[6] just under 10 billion metric tons of greenhouse gases were produced annually as of 2014. Of these there are three major contributors: carbon dioxide, methane, and nitrous oxide. Carbon dioxide is the largest contributor amounting to as much as 76% of the total. In the US however, carbon dioxide accounted for 82% of all the greenhouse gas emissions in 2015.[7] Based on these numbers, carbon dioxide emissions seem to be the main source leading to the greenhouse gas effect and subsequent global warming. The three largest producers of carbon dioxide emissions are power plants, the transportation sector, and industry. By targeting specific functions of these producers, we can develop technologies that can reduce the carbon footprint and hopefully help curb the rise in global temperatures.

One of the specific areas that has the potential to see large changes in energy usage and subsequent emissions is the upgrading of small chain alkanes to alkenes. This process traditionally takes place thermally (eq. 1) or via steam cracking of naptha, liquid petroleum gas, or ethane. Cracking requires large amounts of energy to heat massive crackers to temperatures as high as 900°C. The process is very efficient and continues to see small improvements every 5-10 years. However, newer processes for making small chain alkenes have been under investigation[8,9] and could drastically reduce the operating temperatures. Based on a simple calculation of the energy the reduction of the temperature by 400°C would reduce the amount of CO_2 emissions by roughly 0.65 tons of CO_2 per hour of operation.

$$C_nH_{2n+2} \xrightarrow[700\text{-}900C]{} \text{Alkene} + H_2 \qquad (1)$$

One of the methods being investigated is oxidative dehydrogenation (ODH). Oxidative dehydrogenation is a process in which oxygen is added to the feed stream to partially oxidize the alkane to the alkene and form water as the byproduct (eq 2). The major benefit of this reaction is

the thermodynamics change from endothermic direct dehydrogenation, to exothermic oxidative dehydrogenation. This then allows the reaction to proceed at lower temperatures and atmospheric pressure. Catalysts for this reaction have been in development for decades[10] but have barely begun to reach the threshold of commercial viability.

$$C_2H_6 + O_2 \xrightarrow{\text{Cat.}} C_2H_4 + CO_x + H_2O \quad (2)$$

As of 2014, 134 million tons of ethylene is produced annually worldwide with 25 million tons being produced in the US.[11] In order to become commercially viable, the catalyzed pathways have to produce ethylene at similar rates to that of direct dehydrogenation. Some reports have estimated that the minimum rate to accomplish this is 1 $kg_{C2H4}/kg_{cat.}/hr$.[12, 13] Very few catalysts have been able to reach this rate at temperatures lower than 450°C. Part of the reason for this is that above this temperature direct dehydrogenation also occurs allowing for higher ethylene yields.

The study of catalysis has been under development for hundreds of years and therefore catalysts that require just one metal or metal oxide are well studied and fully characterized. However, in order to further increase activity or selectivity or design new mechanistic pathways, many newer catalysts require an intricate combination of two or more metals. This has led to a combinatorial approach that has seen vast strides in industry.[14,15,16] Even though new catalysts are found quickly and efficiently by this method, the physical and chemical properties of materials created in this manner are not always well understood and further characterization is necessary.

Catalyst preparation and characterization are key principles required to facilitate a rational design of experiments. The preparation of a new catalyst requires an idea of what chemical and physical properties are desired in the chosen reaction process and medium. For

instance, in heterogeneous catalysis the matrix of the reaction exists in two phases. Typically these are a solid and either a liquid or gas. As such, the interaction that occurs at the boundary of these two phases needs to be understood in order to optimize the reaction. This interaction can rely on the physical properties of the material as much as the chemical properties. Before designing a catalyst both properties need to be understood.

Ethane is a small, thermodynamically stable molecule, and as such, requires tremendous amounts of energy (~423kJ/mol) to activate it for a reaction. In order for ethane to react, a C-H bond must first be broken. This can happen through heterolytic cleavage or homolytic cleavage. The latter is a radical reaction that can happen in the gas phase at high temperature and is often the mechanism for direct dehydrogenation. Under the conditions outlined later in the dissertation this is not a likely mechanism of ODH that occurs at such temperatures. Heterolytic cleavage, however, happens via a two-electron process in which a nucleophilic species abstracts a proton.

Transition metals with redox properties are ideal for a heterolytic type of C-H activation and Mo, V, and Ni oxides have all been used to show this reactivity at low temperatures.[17,10] Nickel is very abundant, has a simple two electron redox cycle, and mainly produces CO_2 rather than CO as a side product. For this reason nickel oxide was chosen as the fundamental species for the development of a new catalyst system. Although nickel oxide is very good at activating ethane, it actually is a little too active and ends up overoxidizing ethane, leading to large amounts of combustion. Surface electrophilic oxygen species have been identified as the cause of overoxidation to CO_2. [18,19] These highly active oxygens are a function of nickel vacancies in the lattice that lead to non-stoichiometric Ni_2O_3 clusters in the lattice. The electrophilic oxygen species in these clusters are responsible for the C-H activation that leads to the combustion of both ethane and ethylene.

To reduce the amount of these electrophilic oxygen species, higher valent metal atoms such as Nb, Ti, Mo, and others can be substituted into the lattice of the NiO to keep nickel in its reduced valence state (Ni^{2+}) and limit the number of O^- radicals that lead to combustion. The doping of the higher valent metal facilitates the heterolytic redox cycle mentioned above (Figure 1.1). The first step in the mechanism is likely a concerted C-H activation[20] then a β-Hydrogen elimination and subsequent release of ethylene and water. The catalyst is then reactivated by oxygen. The results of these substitutions give very high selectivity to ethylene.[21-25] However, this can also lead to very low conversion as there are now fewer active oxygens. The lower concentration of active oxygens allows for high selectivity but limits the conversion. In order to overcome this challenge a third metal oxide species can be added to further alter the chemistry in order to facilitate both high selectivity and increased conversion.

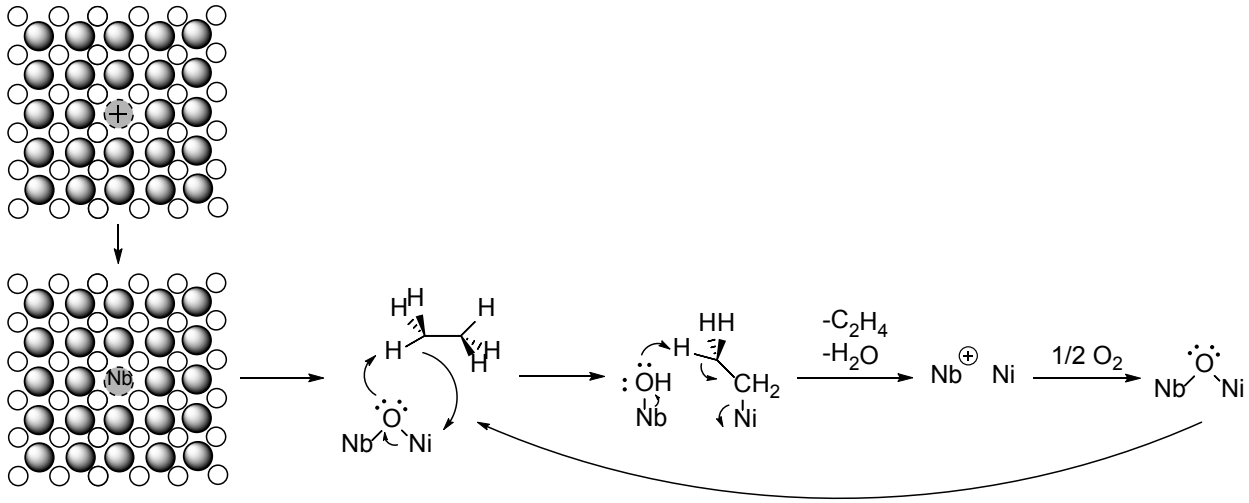

Figure 1.1 Proposed mechanism for doped NiO for ODH of ethane.

The oxygen in the feedstock of the ODH of ethane plays an important role in the competition between the conversion and selectivity. As a result, the desired ternary additive needs to maintain or improve the redox properties of the nickel oxide active site while also maintaining the desired selectivity. Ceria oxide is a good candidate to start with due to its ability

to rapidly uptake and store oxygen.[26] Its' ability, in a partially reduced state, to readily transfer oxygen through its lattice also makes it a good option.[27]

Bulk catalysts are ideal for investigating the physical and chemical properties of a metal oxide in relation to a specific reaction. However, in most cases they are impractical for commercialization. There are two main reasons for this. The first is the cost of using large amounts of expensive metals. The second reason is that bulk materials have very few exposed active sites. In order to scale up these catalysts, active species are supported on inert nanomaterials that have large surface areas where the active material can be dispersed. This facilitates an increase in the number of available active sites and allows for less of the active phase to be used.

This dissertation will outline the role of using various additives and supports for enhancing the role of nickel oxide in the oxidative dehydration of ethane. It will begin with the preparation and characterization of bulk solid solution catalysts and conclude with supported catalysts that are more suitable for industrial applications.

References

1. Delworth, T.L.; Knutson, T.R. Simulation of Early 20th Century Global Warming, *Science,* **2000**, 287(5461), 2246-2250.
2. Root, T.L.; Price, J.T.; Hall, K.R.; Schneider, S.H.; Rosenzweig, C.; Pounds, J.A.; Fingerprints of Global Warming on Wild Animals and Plants, *Nature*, **2003**, 421, 57-60.
3. Laffoley, D.; Baxter, J.M. *Explaining Ocean Warming: Causes, scale, effects and consequences*, Full report. Gland, Switzerland: IUCN. 456 pp.
4. Webster, P.J.; Holland, G.J.; Curry, J.A.; Chang, H.R. Changes in Tropical Cyclone Number, Duration, and Intensity in a Warming Environment, *Science,* **2005**, 309(5742), 1844-1846.
5. Hughes, T.P.; Kerry, J.T.; et.al Global Warming and recurrent mass bleaching of corals, *Nature,* **2017**, 543, 373-377.
6. United States environmental protection agency. https://www.epa.gov/ghgemissions/global-greenhouse-gas-emissions-data (accessed December 1, 2018)
7. Center for Climate and energy solutions. https://www.c2es.org/content/u-s-emissions/ (accessed December 1, 2018)

8. Amghizar, I.; Vanewalle, L.A.; Van Geem, K.M.; Marin, G.B. New Trends in Olefin Production, *Engineering* **2017**, 3, 171-178.
9. Sadrameli, S. M., Thermal/catalytic cracking of liquid hydrocarbons for the production of olefins: A state-of-the-art review II: Catalytic cracking review. *Fuel* **2016,** *173*, 285-297.
10. Gärtner, C. A.; van Veen, A. C.; Lercher, J. A., Oxidative Dehydrogenation of Ethane: Common Principles and Mechanistic Aspects. *ChemCatChem* **2013,** *5* (11), 3196-3217.
11. The essential chemical industry-online http://www.essentialchemicalindustry.org/chemicals/ethene.html (accessed December 5, 2018)
12. Cavani, F.; Ballarini, N.; Cericola, A., Oxidative dehydrogenation of ethane and propane: How far from commercial implementation? *Catalysis Today* **2007,** *127* (1), 113-131.
13. Chu, B.; Truter, L.; Nijhuis, T. A.; Cheng, Y., Performance of phase-pure M1 MoVNbTeOx catalysts by hydrothermal synthesis with different post-treatments for the oxidative dehydrogenation of ethane. *Applied Catalysis A: General* **2015,** *498*, 99-106.
14. Potyrailo, R.; Rajan, K.; Stoewe, K.; Takeuchi, I.; Chisholm, B.; Lam, H., Combinatorial and High-Throughput Screening of Materials Libraries: Review of State of the Art. *ACS Combinatorial Science* **2011,** *13* (6), 579-633.
15. Jandeleit, B.; Schaefer, D. J.; Powers, T. S.; Turner, H. W.; Weinberg, W. H., Combinatorial Materials Science and Catalysis. *Angewandte Chemie International Edition* **1999,** *38* (17), 2494-2532.
16. Kagan, H. B., New screening methodologies or combinatorial chemistry applied to asymmetric catalysts. *Journal of Organometallic Chemistry* **1998,** *567* (1), 3-6.
17. Védrine, J. C., Heterogeneous Partial (amm)Oxidation and Oxidative Dehydrogenation Catalysis on Mixed Metal Oxides. *Catalysts* **2016,** *6* (2), 22.
18. Heracleous, E.; Lemonidou, A., Ni–Nb–O mixed oxides as highly active and selective catalysts for ethene production via ethane oxidative dehydrogenation. Part I: Characterization and catalytic performance. *Journal of Catalysis* **2006,** *237* (1), 162-174.
19. Heracleous, E.; Lemonidou, A., Ni–Nb–O mixed oxides as highly active and selective catalysts for ethene production via ethane oxidative dehydrogenation. Part II: Mechanistic aspects and kinetic modeling. *Journal of Catalysis* **2006,** *237* (1), 175-189.
20. Lin, X.; Xi, Y.; Sun, J., Unraveling the Reaction Mechanism for Nickel-Catalyzed Oxidative Dehydrogenation of Ethane by DFT: The C–H Bond Activation Step and Its Following Pathways. *The Journal of Physical Chemistry C* **2012,** *116* (5), 3503-3516.
21. Savova, B.; Loridant, S.; Filkova, D.; Millet, J. M. M., Ni–Nb–O catalysts for ethane oxidative dehydrogenation. *Applied Catalysis A: General* **2010,** *390* (1-2), 148-157.
22. Zhu, H.; Ould-Chikh, S.; Anjum, D. H.; Sun, M.; Biausque, G.; Basset, J.-M.; Caps, V., Nb effect in the nickel oxide-catalyzed low-temperature oxidative dehydrogenation of ethane. *Journal of Catalysis* **2012,** *285* (1), 292-303.
23. Santander, J.; López, E.; Diez, A.; Dennehy, M.; Pedernera, M.; Tonetto, G., Ni–Nb mixed oxides: One-pot synthesis and catalytic activity for oxidative dehydrogenation of ethane. *Chemical Engineering Journal* **2014,** *255*, 185-194.
24. Zhu, H.; Rosenfeld, D. C.; Anjum, D. H.; Caps, V.; Basset, J. M., Green synthesis of Ni-Nb oxide catalysts for low-temperature oxidative dehydrogenation of ethane. *ChemSusChem* **2015,** *8* (7), 1254-63.
25. Zhou, Q.; Zhou, D.; Wu, Y.; Wu, T., Oxidative dehydrogenation of ethane over RE-NiO (RE=La, Nd, Sm, Gd) catalysts. *Journal of Rare Earths* **2013,** *31* (7), 669-673.

26. Trovarelli, A., Structural and Oxygen Storage/Release Properties of CeO2-Based Solid Solutions. *Comments on Inorganic Chemistry* **1999,** *20* (4-6), 263-284.
27. Saraf, L.; Wang, C. M.; Shutthanandan, V.; Zhang, Y.; Marina, O.; Baer, D. R.; Thevuthasan, S.; Nachimuthu, P.; Lindle, D. W., Oxygen transport studies in nanocrystalline ceria films. *Journal of Materials Research* **2011,** *20* (05), 1295-1299.

Chapter 2: Experimental

The mechanisms and reactivity of heterogeneous catalysts can be much more convoluted than homogeneous organometallic catalysts. Solid catalysts are made up of many tiny crystals that have different lattice planes and multiple types of defects in the crystal itself. This leads to a variety of different sites that may be active or inactive for a specific reaction. In order to gain a reasonable understanding of what is taking place as a reaction proceeds, these materials not only need to be carefully prepared but also need to be well characterized. This section outlines the general preparation, characterization, and reactivity of the catalysts used in this study.

When choosing a method for preparing a heterogeneous catalyst, there are many options involving different variables to choose from.[1] Each of these preparations has an expected a general outcome. However, each step in the process of the method can have a dramatic effect on the physical properties if not performed identically between batches of material. Catalyst synthesis can take a few days to complete. For this reason, it is in the best interest of time to make these materials on a much larger scale than homogeneous catalysts.

In this study 3-4 g of material were prepared in each batch. The large amount of catalyst prepared at once, allows for the use of multiple different characterization techniques, as well as repeated measurements of the activity. In addition, using the same batch of catalyst rules out differences in reactivity due to changes during synthesis batches. The term “bulk” is used to describe a non-supported metal or metal oxide catalyst. Bulk catalysts are used for identifying and investigating the function of the different species of a catalyst made up of more than one component. In contrast, supported catalysts are designed and used more for scale up and industrial applications. In these studies, we will only focus on two methods: a co-precipitation

method involving a structuring agent for the bulk catalyst, and a process called incipient wetness impregnation for the supported catalyst.

The co-precipitation method[2,3,4] is a very simple method in which the catalytically active precursor metal salts are dissolved in water. These metal salts reach an equilibrated homogeneous solution of ions. (This allows for effective distribution of each element throughout the catalysts as it forms a solid solution in the drying step.) The solution is then dried and heated (calcined) in a muffle furnace at temperatures that elicit the desired phase through the decomposition of the metal precursor ions. This temperature is determined by thermogravimetric analysis (TGA). In some of the studies described a structuring agent is added to the solution, which forces a precipitate to form. This structuring agent also enables an extended pore structure, allowing for larger surface areas to be obtained.[5]

A specialized support was used to synthesize nickel oxide on mesoporous alumina[6,7,8,9] catalysts in collaboration with the Woodfield group at BYU. One of the main purposes of using a support for commercial catalysts is the ability to increase the surface area of the active species. These designed silica doped alumina are unique in that they maintain high surface areas and large pore volumes even at elevated temperatures. For this study, only nickel was added without additional metals, to investigate the nickel oxide support interaction in comparison with other aluminas that have previously been tested and reported.[3,10-13]

Nickel oxide was added to the mesoporous aluminas via the incipient wetness impregnation technique.[14] A solution of the nickel salt is dissolved in water at a specific concentration that will give the desired wt% of metal oxide on the support. The solution is added dropwise in matched volumes to the pore volume of each support. This allows the solution to adhesively wick into the pore structure of the support. The outcome of this technique yields the

highest possible distribution of active phase. In order to achieve a large wt% of the active species, multiple impregnations may be necessary. The catalyst is then dried and calcined in a muffle furnace at temperatures determined by TGA.

Characterization of Physical Properties

Once the catalysts were prepared characterization was conducted to verify the synthesis was performed properly. The characterization also helps to clarify any hypothesis regarding reactivity. N_2 physisorption is a standard procedure for characterizing surface area, pore volume, and pore size of the heterogeneous catalysts. The surface area gives both insight into how much active species can be distributed onto the support and also how much of the surface is able to react with the reagents. The pore structure is important in understanding how well the active species or reactants can be distributed in the material. It can also be utilized as the main source of selectivity as is the case for most zeolite composites, which restrict molecular reactivity by shape and size.[15]

The most common equation used for determining surface area is the Brunauer, Emmett, and Teller equation.[16] This equation describes the fraction of volume adsorbed at a specific partial pressure over the volume adsorbed with a monolayer of coverage (eq. 3).

$$\frac{x}{V(1-x)} = \frac{1}{cV_m} + \frac{(c-1)x}{cV_m} \quad (3)$$

In this equation x is P/P_o where P is the partial pressure of nitrogen, and P_o is the saturation at 77K (the temperature of liquid nitrogen). Variable V is the volume of nitrogen adsorbed at a given pressure, whereas V_m is the volume adsorbed with a monolayer of nitrogen. The constant is calculated from a different equation (eq 4-5) :

$$c = c_o \exp\left[\frac{\Delta H_{a_1} - \Delta H_c}{RT}\right] \quad (4)$$

$$c_o = \frac{a_1 b_2}{a_2 b_1} \quad (5)$$

In the equation above (eq. 5) a_1b_2 and a_2b_1 are pre-exponentials for condensation and evaporation. ΔH_{a_1} is the heat of adsorption and ΔH_c is the heat of condensation (eq 4). This equation is in the form of $y = mx+b$ so in order to work up the data one can simply graph $\frac{x}{V(1-x)}$ vs x from which and c and V_m can be calculated from the slope of the line and the intercept. The surface area can then be calculated by assuming the area of N_2 is 0.162 nm^2 and multiplying 4.35*V_m.

Calculating the pore volume and diameter is slightly more complicated and when a cylindrical model of the pore is assumed the method by Barrett, Joyner, Halenda is typically used.[17] Their model uses the desorption branch of the hysteresis loop or isotherm. At each partial pressure the model takes into account two things. The first is the "core" of the pore which represents the condensed N_2 that has evaporated at that specific partial pressure based on the Kelvin equation.[18] Second, despite the "core" of the pore being evaporated there is still some condensed N_2 adsorbed onto the wall of the pore and the thickness of the layer varies and is calculated at each partial pressure. The instrument calculates these individual changes at each partial pressure and summarizes them into a single point value for the pore volume and pore diameter.[19]

In some cases the assumption of a cylindrical pore is not accurate and other models are used in calculating the pore diameters. The shape of the isotherm hysteresis can indicate the presence of different pore structures such as more slit like pores. The change in the hysteresis is typically categorized from H1 to H4. H1 is a standard agglomeration of spherical particles with

cylindrical pore geometry. H2 refers to ink-bottle pores because they have narrow entrances but have relatively uniform channels. H3 are plate like particles that have slit-like pores. H4 are hollow spheres, or particles with internal voids that have irregular shape, or narrow slit-like pores. The silica doped aluminas are H4 and have these slit like pores. As such, another model is used in defining the pore diameter of those supports.[20] An example of the procedure for characterization using nitrogen physisorption is included below.

Procedure for N_2 Physisorption

Approximately 200 mg of material is placed in a sealed glass tube that has been weighed separately from the added powder. The powder is purged of all other gases at 200C for at least 8 hours in an inert gas. The tube is covered with a rubber stopper and cooled to room temperature. A new weight of the tube, powder and rubber stopper together is measured, and from this the actual weight of the sample for calculations is obtained. When this is completed the tube is connected to the instrument and then cooled to 77K in a liquid nitrogen dewar. The partial pressure for nitrogen inside the sealed tube is then increased incrementally and measured after reaching equilibrium at multiple partial pressures. Once the maximum partial pressure is obtained then the partial pressure is decreased incrementally and measured in the same manner. As the nitrogen desorbs, this create a hysteresis loop from which the surface area and pore properties can be calculated.

Another characterization method is powder X-ray diffraction (P-XRD), which is used to define the crystal structure and crystallite size of the active species in catalysis. It can also indicate if the different metal ions in a solid solution have exchanged into the lattice of another

metal or metal oxide. The basic concept of crystallography was outlined in a theory by William Bragg in 1912.[21] In this theory, X-rays are diffracted off a sample at a specific angle. Each parallel plane of the lattice is treated as a mirror reflecting the X-rays (Figure 2.1). As a result each X-ray that reflects off an atom in the plane can interact constructively or destructively. Since the X-rays are interacting with multiple atoms throughout the lattice the reflections obtained are only those that have perfect constructive interference. The Bragg equation defines those reflections that satisfy the conditions where n is any integer of the incident X-ray of a given wavelength = λ. The angle of the incident X-ray is θ and the distance between the parallel planes of the lattice (eq. 6) is the angle of the incident X-ray and d is the distance between the parallel planes of the lattice.

$$n\lambda = 2d \sin\theta \qquad (6)$$

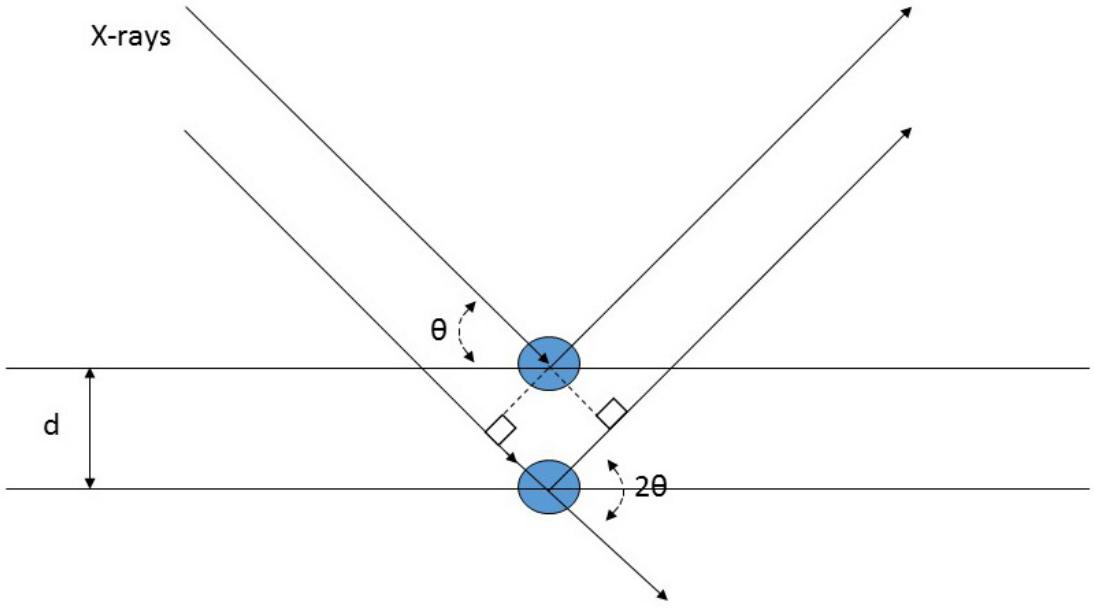

Figure 2.1 Illustration of the geometry used to define Braggs Law.

Unlike single crystal XRD that requires large mm sized long-range crystal structure, the crystals for powder XRD are disordered and on the scale of nm-μm. In order to get structural

data from such small crystals the analysis of the data requires a slightly different approach than that of single crystal XRD. The many different orientations of crystals in a powder sample can blur the diffraction patterns. With ideal fine-grained samples this leads to cones of reflectance or in a 2D format a series of rings with each ring representing a specific plane of the crystal lattice. For this reason many powder instruments are set up with what is defined as a Bragg-Brentano geometry.[22] This is where the detector is placed at a specific distance from the sample and cuts through these rings creating a 1D intensity pattern of the rings or crystal planes. From these planes the lattice structure of the material can be identified and size information can also be obtained. The crystal size can be calculated using the Scherrer equation based on the broadening of the peak (eq. 7).[23]

$$A = \frac{K\lambda}{B\cos\theta} \quad (7)$$

In this equation A is the average crystal size, K is a shape factor that is determined by the software using the full width half maximum (FWHM) of the peaks, λ is the =X-ray wavelength, B is a broadening term, and θ is the angle of the incident X-ray. A sample procedure for using the P-XRD is included below.

Procedure for P-XRD

Powders are prepared in sample holders and analyzed on a PANalytical X'pert Pro MPD diffractometer. The data is worked up using High Scores Plus software. Peak profile fitting is used to identify the size of the crystallites in the material. An ICSD database is used to identify the structure of the crystal. Any ion exchange or lattice parameters are calculated using Rietveld refinement.

Characterization of Chemical Properties

Another characterization method is X-ray photoelectron spectroscopy (XPS), which is an X-ray technique for elemental analysis of materials. It is a quantitative technique that measures the surface of the material to a depth of approximately 10-20nm. It works by irradiating the surface of the material with X-rays and measuring the kinetic energy and quantity of electrons that are emitted. This can provide information about the types of atoms at the surface and the electronic state of those atoms.

The reason XPS is capable of identifying each atom is the electrons in each atom have specific binding energies. Determining the binding energy associated with each atom, and adjusting for the shift in valence state is used to identify the correct oxidation state for a specific species. However, due to the high energy of the incident X-ray, many other peaks can be observed, such as satellite peaks and auger peaks leading to a complicated spectral analysis. Satellite peaks are a function of inelastic scattering of the electron leading to energy loss. Auger peaks are the result of the x-rays ejecting a core electron and that electron subsequently ejecting other valance electrons. These other transitions can be used at times to further identify features of the material such as oxidation state. A sample procedure for XPS analysis is included below.

Procedure for XPS

Samples were prepared by making a fine layer of powder on carbon tape attached to the sample holder. The samples are then analyzed on a Surface Science SSX-100 X-ray photoelectron spectrometer with an Al Kα source (1486.7 eV) and a hemispherical analyzer. Narrow scans were recorded with spot size of 800 um × 800 um, and resolution 4 (nominal pass energy 100 eV), 40 scans, and a step size of 0.065 eV. All peaks were

calibrated with respect to the C 1s peak in the narrow scan at 285 eV binding energy. Peak fitting was performed using CasaXPS software.

Another characterization method is thermogravimetric analysis (TGA), which is a technique that is used to isolate the temperatures at which a phase change in a material occurs as it decomposes from the starting material. These changes can be measured a few different ways. The first is by the change in mass with respect to temperature. As the material decomposes, physisorbed water is released and the mass is reduced. At higher temperatures organic precursor combusts and lattice oxygen is released as water both of which lead to a reduction in the mass. In many cases a mass spectrometer is connected to identify the decomposition products. The other way to measure this change is to measure the voltage change. The decomposition of precursor or the change in phase typically gives off large amounts of energy, and this is reflected as a peak in the voltage. When all of these are combined, the mass loss and change in voltage can be used to specify decomposition or a change in phase of the material, for example from gamma or delta alumina to alpha-alumina. A sample procedure for a TGA experiment is included below.

Procedure for TGA

Approximately 30 mg of material is weighed into an alumina or platinum crucible. The crucible is placed on a sample stand in the instrument. The chamber is evacuated and the ambient gas is chosen depending on the desired outcomes: a metal reduction requires hydrogen while a metal oxidation requires air. Both are used at a flow rate of 20ml/min respectively. While the gas is flowing the temperature is ramped at 10°C/min from 25-1000°C. The sample is then cooled to room temperature.

Another characterization method is chemisorption analysis, which is performed in a very similar manner to the N_2 physisorption outlined above. The main difference is that a reactive gas is used that binds to the surface of the material being investigated. While the information from multilayers of gas are the more important variable for an inert gas the monolayer of gas chemically bound to the surface gives the pertinent information for chemically active surface area.

Dynamic chemisorption can be performed with different reagents. Each reagent can give insight to different aspects of the catalyst. For example hydrogen is used to look at the reducibility of the catalysts whereas ammonia is used to look at the total acid sites available for catalysis or binding. A sample procedure for the hydrogen reduction chemisorption analysis also known as hydrogen temperature programmed reduction is below.

Procedure for H_2-TPR

A plug of quartz wool is placed in a U shaped tube and 100 mg of catalyst are added on top. A quartz insert is added to keep powder from back flushing up into the flow valves. The tube is inserted into a Micromeritics 3 Flex Surface characterization instrument. 10% hydrogen in argon is flowed through the reactor at 50 mL/min. The temperature is ramped from 25-1000°C then cooled to room temperature. A thermal conductivity detector (TCD) is used to measure the signal and the data can be plotted as μV/time or μV/temperature.

In some cases when characterizing nanomaterials, it is difficult to observe a few of the properties of a material by readily available techniques such as powder XRD and XPS. In these cases more advanced X-ray techniques can give insight into these fundamental properties such as

crystallite size below the detection limits of P-XRD, position in the lattice, atom type, and their oxidation states. Two of these techniques utilized in future chapters are extended X-ray absorption fine structure (EXAFS) and X-ray Absorption Near Edge Structure (XANES). Both of these techniques require a synchrotron radiation source in order to produce the intensity of X-rays needed for the analysis.[24]

Both EXAFS and XANES utilize the same process as XPS in that a large amount of X-rays are directed at a material and when the energy of those X-rays matches the energy to overcome the work function of the material for a specific core electron that electron is ejected. This creates an energy profile where the energies of ejected electrons are called the step edges. Due to the high intensity of the X-ray source very distinct step edges can be identified. The area before the edge is called the XANES region that gives information about the local coordination environment or coordination number as well as the oxidation state of an element. The region just after the edge is the EXAFS region, which gives the nearest neighboring atoms and their bond lengths. The data for these experiments were collected and analyzed as part of a collaboration. A sample experimental procedure is below.

Procedure for EXAFS and XANES

The data were collected at QAS beamline of the NSLS-II of Brookhaven National Laboratory and later at the advanced photon source (APS) beamline 20. Ni K edge data were collected in transmission mode and Ce L edge and Nb K edge data were collected in fluorescence mode (PIPS detector). For the analysis at the NSLS-II the powders for example: CeO2 (Ce^{4+}) and Cerium Nitrate hexahydrate standard (Ce^{3+}), the powders/particles were spread onto sticky tape and analyzed. For the samples analyzed at

APS, the powders were mixed with boron nitride and pressed into pellets. The data were collected in fluorescence mode.

Reaction Testing

After the samples have been synthesized and characterized, the catalytic reaction was tested. The experiments are centered on using a plug flow reactor with flow going down through the catalyst to rule out any mass transfer effects. A custom designed plug flow reactor was used to analyze all reactivity and rate data (Figure 2.2). 100 mg of catalyst was weighed and placed in a quartz tube with a quartz frit and a plug of quartz wool. The quartz tube is placed in a tube furnace connected to Swagelok on each end. The gases are passed through the tube at various flow rates using calibrated mass flow controllers. The temperature is adjusted at 50 degree increments between 200-500°C via the furnace which has a thermocouple measuring the temperature of the catalyst bed. After passing through the catalyst the products are measured by online GCMS-TCD to obtain conversion and selectivity data for the reaction.

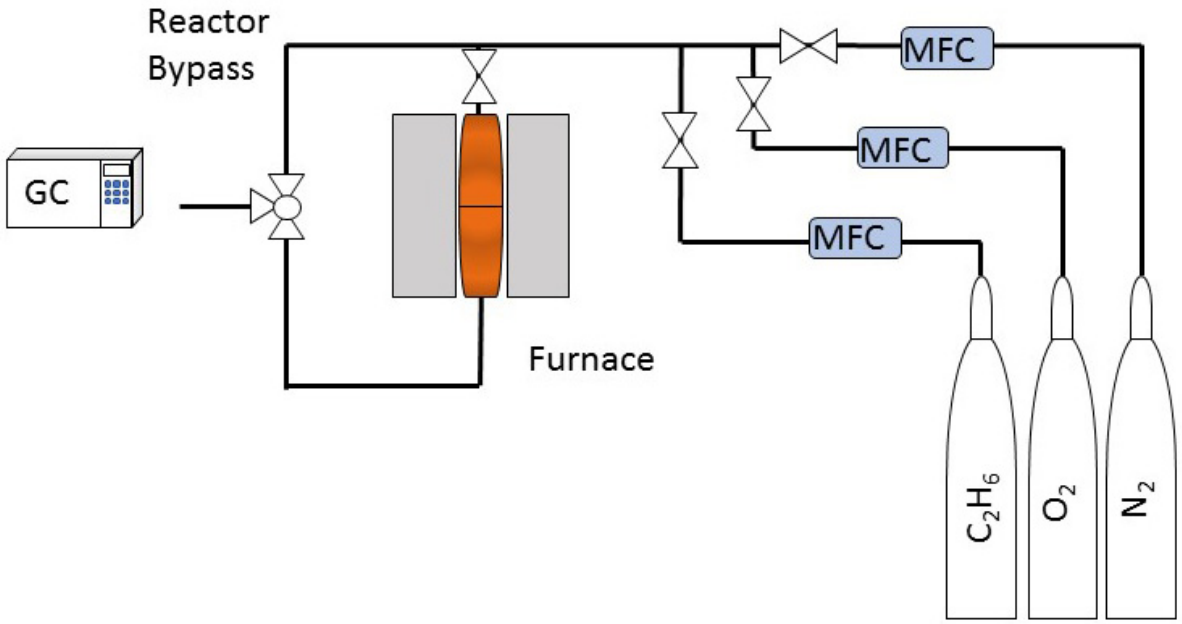

Figure 2.2 Custom plug flow reactor.

References

1. Regalbuto, J., *Catalysts Preparation Science and Engineering*; CRC Press: Boca Raton, FL, 2007.
2. Kolthoff, I. M., Theory of Coprecipitation. The Formation and Properties of Crystalline Precipitates. *The Journal of Physical Chemistry* **1931,** *36* (3), 860-881.
3. Heracleous, E.; Lee, A.; Wilson, K.; Lemonidou, A., Investigation of Ni-based alumina-supported catalysts for the oxidative dehydrogenation of ethane to ethylene: structural characterization and reactivity studies. *Journal of Catalysis* **2005,** *231* (1), 159-171.
4. Heracleous, E.; Lemonidou, A., Ni–Nb–O mixed oxides as highly active and selective catalysts for ethene production via ethane oxidative dehydrogenation. Part I: Characterization and catalytic performance. *Journal of Catalysis* **2006,** *237* (1), 162-174.
5. Solsona, B.; Concepcion, P.; Hernández, S.; Demicol, B.; Nieto, J. M., *Oxidative dehydrogenation of ethane over NiO–CeO 2 mixed oxides catalysts*. **2012**; Vol. 180.
6. Huang, B.; Bartholomew, C. H.; Smith, S. J.; Woodfield, B. F., Facile solvent-deficient synthesis of mesoporous γ-alumina with controlled pore structures. *Microporous and Mesoporous Materials* **2013,** *165*, 70-78.
7. Huang, B.; Bartholomew, C. H.; Woodfield, B. F., Facile structure-controlled synthesis of mesoporous γ-alumina: Effects of alcohols in precursor formation and calcination. *Microporous and Mesoporous Materials* **2013,** *177*, 37-46.
8. Huang, B.; Bartholomew, C. H.; Woodfield, B. F., Facile synthesis of mesoporous γ-alumina with tunable pore size: The effects of water to aluminum molar ratio in hydrolysis of aluminum alkoxides. *Microporous and Mesoporous Materials* **2014,** *183*, 37-47.
9. Mardkhe, M. K.; Keyvanloo, K.; Bartholomew, C. H.; Hecker, W. C.; Alam, T. M.; Woodfield, B. F., Acid site properties of thermally stable, silica-doped alumina as a function of silica/alumina ratio and calcination temperature. *Applied Catalysis A: General* **2014,** *482*, 16-23.
10. Zhang, X.; Gong, Y.; Yu, G.; Xie, Y., Oxygen species on NiO/Al2O3 and their reactivities. *Journal of Molecular Catalysis A: Chemical* **2002,** *180* (1), 293-298.
11. Zhang, X.; Liu, J.; Jing, Y.; Xie, Y., Support effects on the catalytic behavior of NiO/Al2O3 for oxidative dehydrogenation of ethane to ethylene. *Applied Catalysis A: General* **2003,** *240* (1), 143-150.
12. Smoláková, L.; Botková, Š.; Čapek, L.; Priecel, P.; Sołtysek, A.; Kout, M.; Matějová, L., Precursors of active Ni species in Ni/Al2O3 catalysts for oxidative dehydrogenation of ethane. *Chinese Journal of Catalysis* **2013,** *34* (10), 1905-1913.
13. Skoufa, Z.; Xantri, G.; Heracleous, E.; Lemonidou, A. A., A study of Ni–Al–O mixed oxides as catalysts for the oxidative conversion of ethane to ethylene. *Applied Catalysis A: General* **2014,** *471*, 107-117.
14. Haukka, S.; Lakomaa, E. L.; Suntola, T., Adsorption controlled preparation of heterogeneous catalysts. In *Studies in Surface Science and Catalysis*, Dąbrowski, A., Ed. Elsevier: 1999; Vol. 120, pp 715-750.
15. Turkevich, J., Zeolites as Catalysts.I. *Catalysis Reviews* **1968,** *1* (1), 1-35.

16. Brunauer, S.; Emmett, P. H.; Teller, E., Adsorption of Gases in Multimolecular Layers. *Journal of the American Chemical Society* **1938,** *60* (2), 309-319.
17. Barrett, E. P.; Joyner, L. G.; Halenda, P. P., The Determination of Pore Volume and Area Distributions in Porous Substances. I. Computations from Nitrogen Isotherms. *Journal of the American Chemical Society* **1951,** *73* (1), 373-380.
18. Thomson, W., LX. On the equilibrium of vapour at a curved surface of liquid. *The London, Edinburgh, and Dublin Philosophical Magazine and Journal of Science* **1871,** *42* (282), 448-452.
19. Micromeritics Tristar II instrument manual.
20. Huang, B.; Bartholomew, C. H.; Woodfield, B. F., Improved calculations of pore size distribution for relatively large, irregular slit-shaped mesopore structure. *Microporous and Mesoporous Materials* **2014,** *184*, 112-121.
21. Bragg, W. H.; Bragg, W. L., The reflection of X-rays by crystals. *Proceedings of the Royal Society of London. Series A, Containing Papers of a Mathematical and Physical Character* **1913,** *88* (605), 428-438.
22. Dinnebier, R.E.; Billinge, S.J.L. *Powder diffraction theory and practice,* RSCPublishing: Cabridge, U.K., 2008. pp1-19.
23. Patterson, A. L., The Scherrer Formula for X-Ray Particle Size Determination. *Physical Review* **1939,** *56* (10), 978-982.
24. Iwasawa, Y.; *X-ray absorption fine structure for catalysts and surfaces,* World Scientific Publishing Co. Pte. Ltd.:River Edge, NJ. 1996.

Chapter 3: Low Temperature Oxidative Dehydrogenation of Ethane by Ce Modified NiNb Catalysts

Adapted from published article in *Ind. Eng. Chem. Res.,* **2018**, 57, 5234–5240

DOI: 10.1021/acs.iecr.8b00531

Abstract

Low temperature oxidative dehydrogenation catalysts are becoming a viable material for drastically altering the production of small chain alkenes. Among materials used, bi- and tri-metallic nickel catalysts have shown great promise. In this study, we report a 38% increase in the rate of ethylene production with the addition of Ce to NiNb catalysts. Oxidative dehydrogenation of ethane was performed in the temperature range of 250-350 °C. At 300 °C, the rate of ethylene production was maximized with a rate of 6.91×10^{-4} mmol$\cdot g_{cat}^{-1} s^{-1}$. At higher temperatures, the rate of deep oxidation to CO_2 outcompeted the rate of ethylene formation. The improved rate due to the addition of Ce is attributed to ceria's ability to rapidly transport oxygen to the NiO active sites.

Introduction

The conversion of ethane to ethylene is a vitally important process and is critical to manufacturing polyethylene and many other chemicals made worldwide.[1] The well-studied homogeneous thermal dehydrogenation reaction has been essential and continues to be implemented. However, an alternative heterogeneous catalytic oxidative dehydrogenation (ODH) reaction has seen vast strides in recent years.[2] In this alternative reaction, oxygen is implemented as a co-feed in the presence of a catalyst to improve the C-H activation of the alkane. This drastically reduces the activation energy of this process and allows conversion of small chain alkanes to proceed at lower temperatures and at higher rates.

The oxidative dehydrogenation of ethane has the potential to replace current ethane cracking methods; consequently, many catalysts have been investigated[3] for efficiency and selectivity. The two most-promising catalysts are a molybdenum-based mixed oxide and a nickel oxide catalyst. The M1 phase catalyst,[4,5] a molybdenum-based oxide that has been investigated extensively in the last 10 years,[6] is currently the most efficient, but suffers from the use of expensive metals and from difficult hydrothermal preparation. Nickel oxide catalysts, on the other hand, are inexpensive, much more abundant,[8] and have simple preparations.[9,10]

A few different variables are reportedly key to improving the efficiency of a nickel catalyst towards ethylene production, with the foremost being a highly acidic additive metal that limits the concentration of electrophilic O^{2-} and O^{-} oxygen species.[11] This property of the catalyst leads to much higher selectivities than the NiO catalyst itself. Large surface areas and small nickel crystallites also improve conversion.[12] In order to improve these properties of nickel catalysts, many additives have been tested for their effects.[3] Among these, niobium has shown great promise.[13-17]

The addition of niobium to nickel reduces the number of nonselective oxygen species on the surface of the catalyst, limiting formation of undesired CO_2.[7,12] This has been shown to give selectivities upwards of 90% at low conversion.[7] Similar to many other additives, niobium has been shown to reduce the nickel crystal size as the amount of additive increases.[12] The maximum amount of niobium that can be exchanged in the crystal lattice before blocking the nickel active sites was found to be a 0.176 Nb-Ni ratio.[7]

The recent strides toward achieving high selectivities have been extremely successful, and the primary attribute that remains to be improved is the low-temperature conversion of these NiNb catalysts. Mechanistic calculations using DFT for ODH of ethane over nickel catalysts

indicate that C-H activation is the rate-limiting step[18-20] for the reaction. In order to improve the conversion, one would either need to remove the electrophilic oxygen available or increase the rate at which the active oxygen species becomes available. An early attempt at the former was investigated with a NiNbTa catalyst, which showed 11.7% conversion and 80.4% selectivity at 300°C,[21] almost doubling the conversion of the nickel catalyst alone.

Ceria is a prime candidate to investigate an increase in oxygen availability at the redox site. Ce is known for its unique oxygen transport and redox properties,[22] and is used often in high temperature combustion to oxidize CO to CO_2 due to its rapid uptake and storage of O_2, e.g., in the three-way catalytic converters in automobile exhaust systems.[23] The oxygen transport properties exhibited by ceria make it an excellent choice in the attempt to improve the ambient O_2 uptake and ultimately the rate of ethylene production. Recent reports of the NiCe catalyst show that this is, in fact, the case at low temperatures.[24]

We report here an investigation of the effect of combining the benefits of the Ce and Nb in a NiO catalyst. The study was motivated by the hypothesis that the oxygen transport properties of Ce would improve the redox properties of the catalyst and therefore improve the rate at which stoichiometric oxygen species are available. As an additive, Nb fills the cationic vacancies, stabilizing the Ni^{2+} species and reducing the amount of nonselective oxygen species, thereby increasing selectivity. Both of these effects in conjunction were hypothesized to improve the overall rate of ethylene production. Catalysts were investigated in the range of 250-350°C in order to assess the performance at low temperature.

Experimental

Catalysts were synthesized by adding 8.24 mmol nickel nitrate (Fisher Scientific certified grade) to 50 mL of 200 proof ethanol (Fisher Scientific). The solution was stirred for 3 minutes;

then 0.05, 0.22, 0.44, and 0.77 mmol ceria nitrate (Alfa Aesar 99.5%) was added to each catalyst, respectively, and stirred for 2 minutes. A standard amount of niobium oxalate (1.76 mmol Alfa Aesar) was added last and the solution was stirred at 400 rpm at room temperature for 10 minutes. The solution changed from clear green to a milky blue. The solution was then evaporated at its boiling point for 30 minutes, followed by cooling to room temperature, and then dried under ambient atmosphere at 100 °C in an oven for 24 hours. The resulting precipitate was then calcined in stagnant air by ramping the temperature at 3 °C/min to 370 °C and held for 2 hours. The NiNb control was prepared in the same manner without the addition of Ce. Catalysts are referred to as XCeNiNb, where X is the wt% of ceria added relative to the constant 17.6 at% of Nb in the NiNb catalyst. The remaining metal content in each catalyst was Ni, for an expected range of 67.4 to 82.4 at% Ni in the prepared catalysts.

X-ray diffraction measurements were taken using a PANalytical X'pert Pro MPD diffractometer with a Cu sealed tube X-ray source ($\lambda(K\alpha) = 0.154$ nm) and a germanium Kα monochromator. The diffraction patterns were taken in the 2θ range of 10-120° with 0.008 step size and a scan rate of 0.0054°/s. PANalytical High Scores Plus software was used to analyze the diffraction patterns and the Scherrer equation was used to calculate the crystallite sizes of the nanoparticles.

CeNiNb samples were digested in concentrated nitric acid (68-70 w/w%) for 48 hours then diluted to 2 ppm (Ce, Ni, Nb total) range with 2 w/w% nitric acid. The samples were analyzed on a Perkin-Elmer Optima 8300 ICP-OES, and the 0.5CeNiNb sample was repeated using an Agilent 7800 ICP-MS.

Surface area and pore volumes were acquired using a Micromeritics TriStar II surface area and porosity instrument. Samples were degassed in N_2 for 24 hours and then analyzed by

multipoint BET analysis under N_2 at 77K. A Slit Pore Geometry model25 was used to analyze the adsorption curves for pore size distribution.

X-ray photoelectron spectroscopy (XPS) was performed using a Surface Science SSX-100 X-ray photoelectron spectrometer with an Al Kα source (1486.7 eV) and a hemispherical analyzer. Narrow scans were recorded with: spot size 800 um × 800 um, resolution: 4 (nominal pass energy 100 eV), the number of scans: 40, and step size: 0.065 eV. All peaks were calibrated with respect to the C1s peak in the narrow scan to 285 eV binding energy. Peak fitting was performed using CasaXPS software.

Thermal gravimetric analysis (TGA) was performed during reduction using a Netzsch STA 409 PC. The calcined samples were heated from 30 °C to 800 °C at a rate of 10 °C/min in a flow of 10% H_2 in N_2.

The CeNiNb catalysts were evaluated in a custom-built flow reactor (Figure 3.5) at atmospheric pressure in a Mellen temperature controlled furnace with an Omega CN7800 temperature controller. 100 mg of catalyst mixed with 1 g of SiC was inserted into a quartz tube reactor (ID of 10 mm). Gas mixtures were introduced into the reactor at a total flow of 10 mL/min. The ratio of the gas was 20% C_2H_6 (99.999%), 10% O_2 (99.99%), and 70% N_2 (99.98%) (W/F = 0.6 g s/mL). The furnace was ramped from room temperature to 250°C at 15°C/min, and experiments were conducted at 50 °C increments to 350 °C after holding at each temperature for an hour. During this time, 4 GC samples were taken at each temperature and averaged to give the values in this report. Reaction gas mixtures were analyzed with an in-line Shimadzu GCMS-QP 2010 equipped with a TCD detector and two columns: a Restek HAYSEP R column and a Supelco Carboxen 1006 PLOT column. The TCD detector was calibrated using

a TOGAS standard and reported signal correction factors.[26] Ethane conversions and ethylene selectivities were calculated on a carbon basis.

Results and Discussion

An adapted method[24] was used for the preparation of the CeNiNb catalyst that showed promise at low temperatures. Niobium was added to the mixture in order to obtain higher selectivities. TGA analysis (Figure 3.6) showed that the catalyst was fully oxidized by 400°C. In order to limit crystallite size of the active material, catalysts were calcined at 370°C for 2 hours. This led to large surface areas and very small crystallite sizes (Table 3.1).

N_2 adsorption was used to investigate the surface areas and pore volumes of the CeNiNb catalysts. The surface areas are large (128-158 m^2/g) and exceed all those previously reported, which are typically in the range of 40-80 m^2/g,[7,14,16] except for NiNb prepared by sol-gel synthesis, which are as large as 225 m^2/g.[14] The CeNiNb surface areas in this report are similar to those prepared by a grinding method with 15 wt% Nb.[27] The reason for this similarity may be due to using oxalic acid as the same structuring agent.

It is interesting, however, that there seems to be no correlation between the surface area and the amount of Ce present. In the preparation of the catalyst, the Ni^{2+} and Ce^{4+} should have reacted with oxalic acid at relatively similar rates, allowing for potential atomic exchange in the lattice as the Nb has been shown to do. However, the size of the Ce atom appeared to limit such exchange and extrude the Ce to the surface. Solsona et al. showed that the Ce does not assimilate into the lattice of the NiO crystal structure.[24] This suggests that the Ce exists either on the surface or in the pore network of the structure and may be the reason why no correlation exists between the general structure of the catalyst and the Ce amount.

Table 3.1 N2 adsorption data and calculated crystallite sizes from XRD data.

Catalyst	BET Surface area (m^2/g)	Pore volume (cm^3/g)	Pore Diameter (nm)	NiO Crystallite size (nm)	CeO_2 Crystallite size (nm)
NiNb	158.3	0.79	38.8	6	N/A
0.5CeNiNb	136.9	0.60	48.8	6	<1
2CeNiNb	128.0	0.63	50.5	6	<1
4CeNiNb	134.9	0.64	46.3	6	<1
15CeNiNb	133.2	0.67	43.6	5	3

The CeNiNb catalysts were analyzed by powder XRD to identify each phase and to define the specific crystallite sizes of each metal oxide. Figure 1 shows the diffraction patterns for each of the CeNiNb catalysts and their comparison to the reference materials of NiO and CeO_2. The NiO peaks for 0.5-15CeNiNb match the reference material for cubic NiO and the NiO crystallites exhibit a consistent size of 6 nm for 0.5-4% Ce additive (Table 3.1). For the 15% catalyst, the NiO size slightly decreased, giving a NiO crystallite size of 5 nm. In the 15CeNiNb sample, the Ce peaks begin to show defined long-range structure that correlates with the CeO_2 reference material and a crystallite size of 3 nm. In order to quantify the amount of ceria present, ICP analysis was performed and the amount of Ce was within 5% of the calculated values for the 2-15% samples (Table 3.5). The XRD analysis can only detect those phases that are crystalline and within the detection limits. The broad peak from 20-33° 2θ for the samples with 0.5-4% Ce additive, is difficult to assign to either ceria or niobium oxide. We would expect Ce to be amorphous and highly dispersed at such low additive loadings. Niobium is known to exchange into the lattice of the NiO[7] and is also accounted for in this broad peak. According to previous studies involving NiNb, niobium exists as amorphous Nb_2O_5 and $NiNb_2O_6$.[27,28] Based on XPS data (Figure 3.7) the major Nb species was found to be amorphous Nb_2O_5.

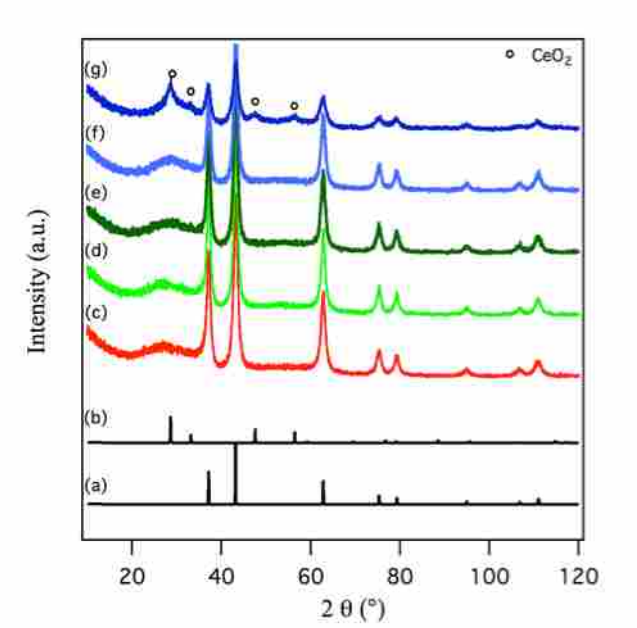

Figure 3.1 XRD diffraction data for CeNiNb catalysts. (a) NiO control, (b) CeO_2 control, (c) NiNb, (d) 0.5CeNiNb, (e) 2CeNiNb, (f) 4CeNiNb, (g) 15CeNiNb.

XPS analysis was performed on the NiNb, 0.5CeNiNb, and 15CeNiNb samples (Figure 3.2) after ODH reaction. The peak for NiO $2p^{3/2}$ in the 0.5CeNiNb and 15CeNiNb samples is centered at B.E. 854 eV and is slightly shifted compared to 853.6 in the NiNb sample.[29] This electronic shift suggests that the Ce promotes a higher valence Ni species either due to a NiNb lattice restructuring[28] or through a direct effect on the Ni itself. Further investigation of the local structure and characterization of these effects is currently in progress. After referencing the peaks and fittings to the NiNb sample, the Ce was then fitted and analyzed. The ceria peaks are assigned to be Ce^{4+} peaks representing the CeO_2 species[30,31] in both samples at 881.8 eV; however, there is only a small contribution in the 0.5CeNiNb sample that is barely identifiable by this technique. O 1s peaks correlate well with all metal oxides and the CeO_2 peak increases in intensity between the 0.5CeNiNb sample and the 15CeNiNb sample as expected (Figure 3.8). There is an extra peak in the 15CeNiNb sample centered at 533.6 eV which correlates to a C-O bonded species. Further analysis of the carbon peak at 287.2 eV suggests that carbonates that

have formed as a result of surface carbon deposition[32] during the catalytic reaction (Figure 3.9). Due to overlapping Ce at the Nb 5d region, Nb 3p was used to identify the niobium that was found to be mainly Nb_2O_5 (Tables 3.5-3.7).

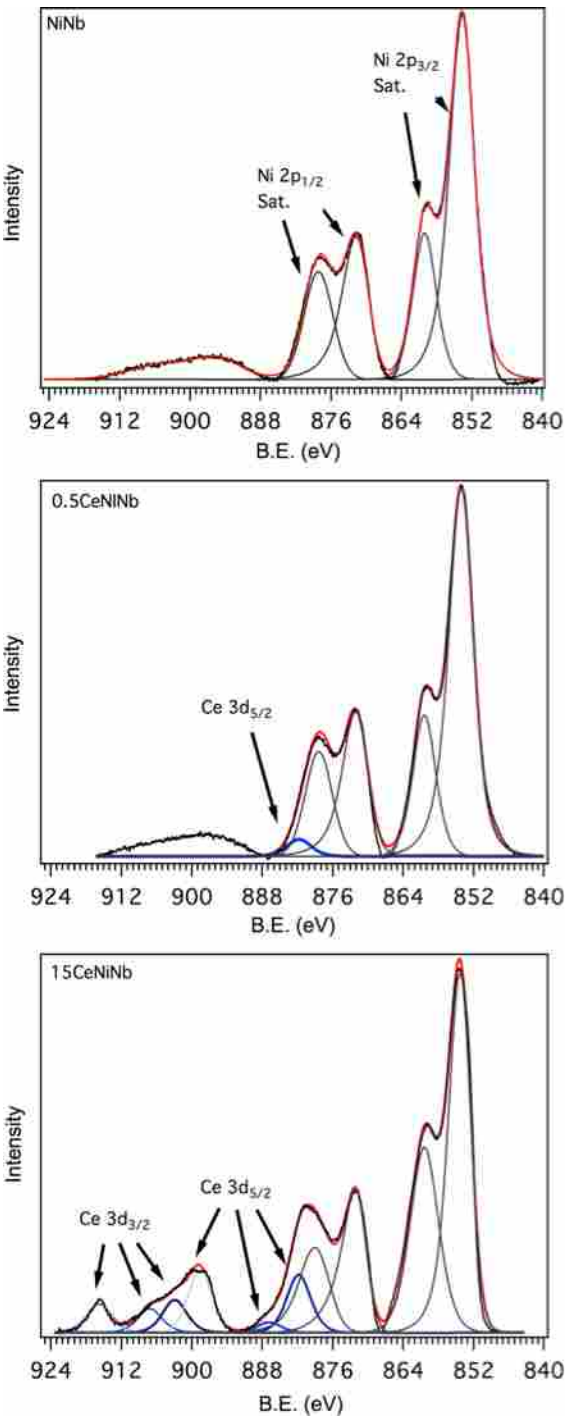

Figure 3.2 XPS Spectra of Ni and Ce regions for NiNb, 0.5CeNiNb, and 15CeNiNb post reaction.

The NiO crystallite sizes and surface areas reported in the literature vary significantly based on the preparation method and the amount of additive introduced. NiO crystallite sizes typically are in the range of 10-20 nm.[11] However, in some cases when additive amounts exceeded 10-15 wt%, the nickel crystal aggregation is limited and smaller nanoparticles are formed.[33] The sizes exhibited in the present study are some of the smallest NiO crystallite sizes observed to date for nickel ODH catalysts, and may be a contributing factor in the conversion rates. The biggest factor in the size of the crystallites is likely the low temperature calcination step in the preparation method. Low-temperature calcination of materials is known for limiting the aggregation of particles during thermal treatment.[33,34]

The reactivity of the CeNiNb catalysts were tested in the range of 250-350°C for low-temperature effects of Ce. The calculated rates and selectivities are presented in Table 3.2. At 250°C, the catalysts showed very minor deviations in conversion from the NiNb standard prepared after the same manner. At this temperature however, a large increase in the selectivity toward ethylene was seen with small additions of ceria. As larger amounts of ceria were added to the catalyst, a linear decrease in selectivity was observed. At 300°C, the conversion increased by approximately 3% with the 0.5CeNiNb sample. After this jump, the conversion decreased for the 2CeNiNb sample and gradually increased with further addition of ceria. The increase in selectivity at 300°C for the NiNb to the 0.5CeNiNb was smaller compared to the increase at 250°C, and followed a volcano type decrease in selectivity as more Ce was added. At 350°C, the conversions increased by 2-3 times with a moderate decrease in the selectivity (Table 3.8).

Table 3.2 Conversion, selectivity, and activation energies of CeNiNb catalysts from 250-300°C.

Catalyst	250°C		300°C		E_a (kJ/mol)	
	$X(C_2H_6)$	$S(C_2H_4)$	$X(C_2H_6)$	$S(C_2H_4)$	C_2H_4	CO_2
NiNb	2.4	56.6	11.7	64.3	69.3	68.4
0.5CeNiNb	3.0	65.4	14.5	65.4	61.7	71.0
2CeNiNb	2.4	63.5	11.6	66.2	61.2	69.8
4CeNiNb	2.7	59.7	13.2	59.9	61.9	71.7
15CeNiNb	3.9	49.1	18.6	48.6	72.8	73.8

*W/F = 0.6 g_{cat}· s/mL, 20% C_2H_6 10% O_2 70% N_2 composition

The addition of Ce to the NiNb had the potential to reduce the selectivity[24] which was observed to a certain extent. However, this decrease was not significant until large amounts of Ce were introduced. It could also be the case that Ce begins to block the active sites of nickel oxide when significant amounts of Ce are added. The slight increase in conversion of the 0.5% Ce may indicate an alternate activation method at the surface due to the very small amount of ceria near the active NiO sites. Ceria with clusters of oxygen vacancies can exhibit much faster redox cycles than isolated oxygen vacancies,[35] the former of which would be present in highly dispersed amorphous ceria. A recent study showed that the reducibility of NiO on Ce-ZrO supports is limited by the rapid oxygen transfer of CeO_2 to NiO.[36] In the reducing environment of methane, NiO was only reduced after all of the CeO_2 had been reduced to Ce_2O_3. In the presence of oxygen however, even small amounts of ceria are known to rapidly uptake and transfer oxygen.[35] In the present study, the increased activity may be due to the rapid transfer of oxygen from ceria to nickel oxygen vacancy sites, closing the redox cycle, and allowing the reaction rate to increase.

The activation energies of both CO_2 and ethylene were calculated using the Arrhenius equation. The activation energy for ethylene formation (produced by the ODH reaction) was

significantly lower than the value for CO_2 formation (produced by both product and reactant oxidation reactions) for the 0.5-4% CeNiNb samples, indicating that the selectivity should favor ethylene production over the deep oxidation products at lower reaction temperatures. Conversely, the 15CeNiNb catalyst exhibited an ethylene reaction activation energy very similar to that of the CO_2 formation reactions, suggesting that selectivity should not be a strong function of temperature at Ce additions greater than 15%.

The specific rate of a reaction is generally a better method to compare the performance of different catalytic materials than conversion. As such, ethylene production rates were calculated at 300°C. In all cases, ceria addition increased the rate of ethylene formation relative to the base NiNb catalyst, as shown in Figure 3.3, with the 0.5% Ce exhibiting the highest rate of ethylene production. Similar rate effects due to small amounts of rare earth oxide (REO) addition have previously been reported for other catalysts undergoing redox cycles.[37] In strict parallel to the present study, ~0.5 wt% REO (lanthana) addition increased the rate of reaction (water gas shift) by up to 30% relative to the unmodified (Fe/Cr/Cu oxide) catalysts, and the rate effect decreased with further REO addition.[33] The observed ODH reaction rates in the present study form a similar "volcano plot", although the 15% Ce catalyst breaks this trend, perhaps due to a modified mechanism as bulk CeO_2 species form, which is suggested by the increase in ODH reaction activation energy and decreased ethylene selectivity for this catalyst. The large (~38%) increase in rate with minor (0.5 wt%) ceria addition could be due to oxygen donation effects previously discussed or it may be related to more subtle electronic effects that modify the ease of completing the required Ni/Ni^{2+} redox cycles.

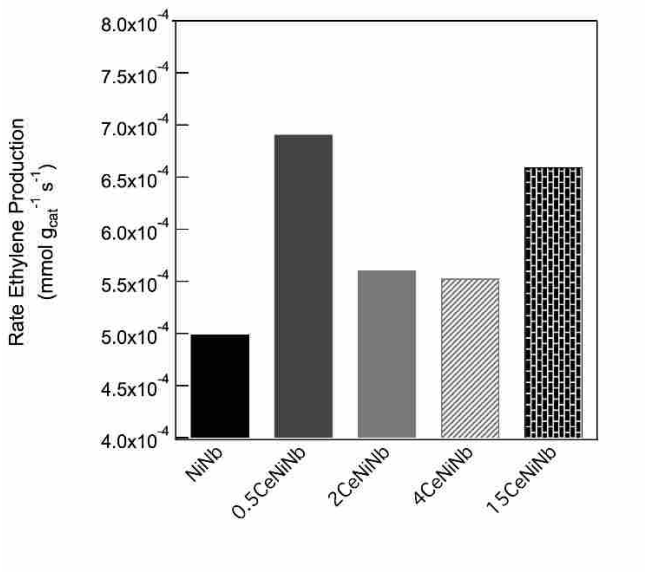

Figure 3.3 Ethylene production rates for CeNiNb catalysts.

Next, we compared the performance of the 0.5CeNiNb catalyst with previous reports for NiNb ethylene production. The Basset group prepared a NiNb catalyst via sol-gel preparation in which citric acid was used as the structuring agent.[14] This sol-gel method produced catalysts with very large surface areas and good atomic exchange of Nb into the NiO crystal lattice. The Lemonidou group prepared catalysts by a co-precipitation method, with the best performance obtained when a 0.176 Nb-Ni ratio was achieved.[7] The Basset group later prepared another NiNb catalyst by a grinding method.[27] This catalyst was the highest performing nickel catalyst of those investigated at 400°C as measured by ethylene yield; however, at 300°C, it showed only marginal performance. In Table 3.3, the parameters of three previous NiNb studies are outlined. The ethane to oxygen feed ratio has typically been 1:1 although one report used a 2:1 feed ratio as in this present study. The catalyst mass to flow rate (W/F) ratio is 0.6 g · s/mL for all except the Lemoniou et. al. data. All experiments are based on 100 mg catalyst samples. Flow rates and conversions were used to calculate the specific rates in mmol g_{cat}^{-1} s^{-1}.

Table 3. 3 Reaction conditions and performance data of previously reported data compared with current study.

Catalysts	% C_2H_6 (C_2H_6/O_2 ratio)	W/F (g·s/mL)	Conv. (%)	Sel. (%)	C_2H_6 Rate (mmol/g_{cat}/s)	C_2H_4 Rate (mmol/g_{cat}/s)
2006Lemonidou NiNb0.176	9.1 (1:1)	0.54	1	90	3.23×10^{-4}	2.90×10^{-4}
2012Basset NiNib0.15	10 (2:1)	0.6	4.8	86	1.29×10^{-4}	1.11×10^{-4}
2015Basset* NiNb0.15	10 (1:1)	0.6	20	76	7.09×10^{-4}	5.39×10^{-4}
0.5CeNiNb	20 (2:1)	0.6	15	65	10.6×10^{-4}	6.91×10^{-4}

All values are calculated from tables or figures within the references based on 0.1 g of catalyst reported.
*"second light off" of catalyst used

The addition of Ce to NiNb catalysts produced improvements in the rate of ethylene production in comparison to the previously reported NiNb catalysts, as illustrated in Figure 4. Preliminary results indicated that increasing the feed ratio to 2:1 ethane: oxygen from 1:1 increases the selectivity significantly, while decreasing the conversion. This observation supports the hypothesis that the ceria is actually transporting the oxygen to the nickel active sites and that ethane is the limiting reagent at the surface. Again, it is noteworthy that only small amounts of Ce were necessary to accomplish this improvement.

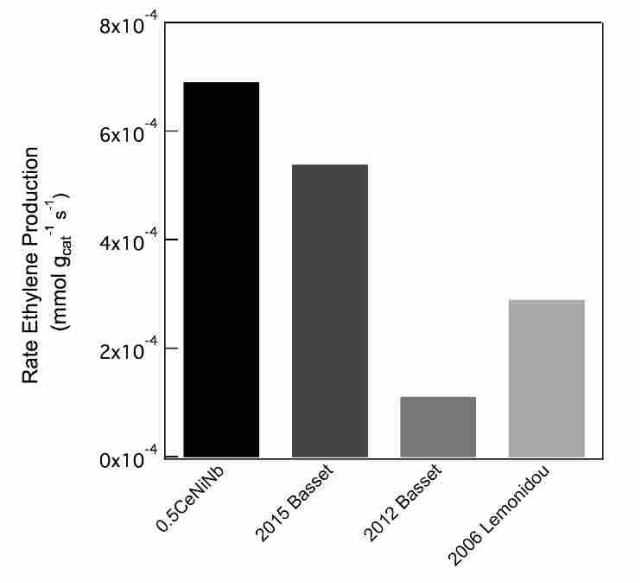

Figure 3.4 CeNiNb ethylene production rates compared with rates from literature.

Conclusions

In this report, we have demonstrated that the addition of Ce to NiNb catalysts slightly decreases the activation energy required to produce ethylene during oxidative dehydrogenation. This, in turn, can improve the rate of ethylene production at 300°C. The precipitation method used to prepare the catalyst produces extremely small NiO crystal sizes which help improve the overall conversions. We also report that only minor amounts of Ce are required to outperform previously reported NiNb catalyst. However, the mechanism by which the 0.5CeNiNb operates is still unclear and further investigation is currently ongoing in order to understand this anomaly.

SI Data

Figure 3.5 Flow reactor setup.

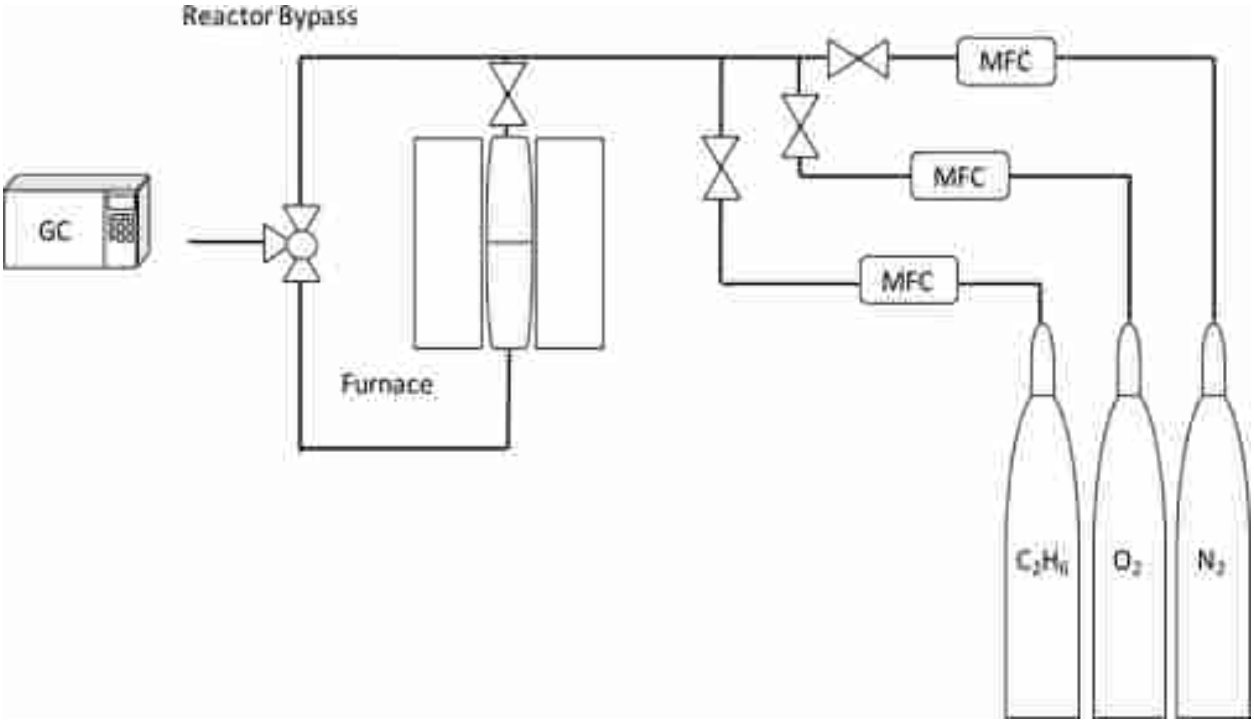

Figure 3.6 TGA analysis of CeNiNb.

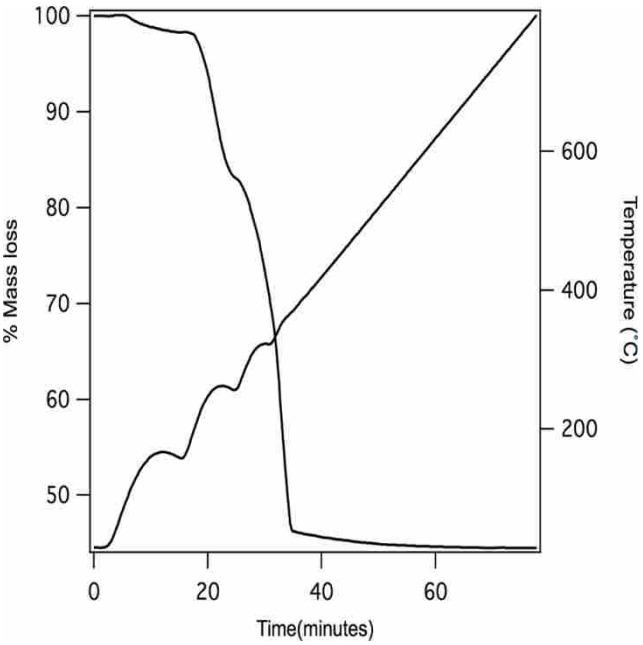

Table 3.4 ICP-OES/ ICP-MS results for nickel and ceria.

Catalyst*	%Ni	%Ce
NiNb precipitate	100	0
0.5CeNiNb	99	1.2**
2CeNiNb	98	1.9
4CeNiNb	96	4.2
15CeNiNb	75	15.1

* Niobium did not dissolve under normal ICP preparation and was not included in this measurement

** Initial ICP-OES measurements put 0.5% Ce in baseline of data. This sample was reanalyzed by ICP-MS with a LOD in the ppb range and the Ceria content was found to be 0.5%

Figure 3.7 XPS data for Nb 3p3/2 of the NiNb, 0.5CeNiNb, and 15CeNiNb samples. The NiNb and the 0.5CeNiNb samples exhibited similar peaks containing Nb_2O_5 and NbO.

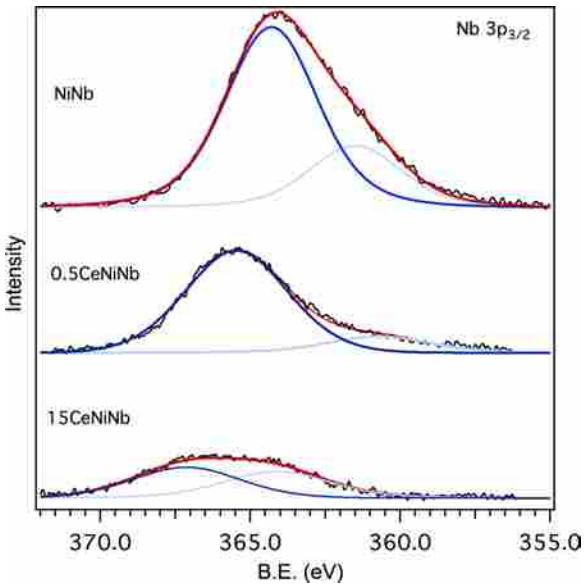

Figure 3.8 XPS O 1s peak for NiNb, 0.5CeNiNb, and 15CeNiNb samples.

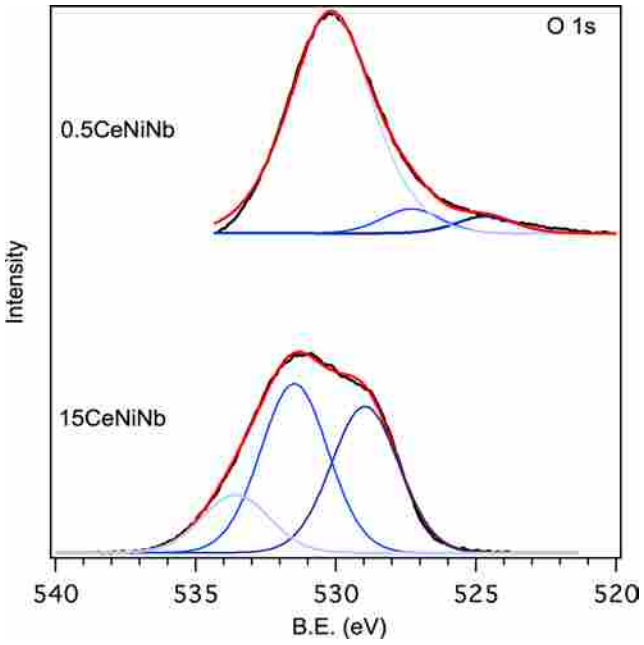

Figure 3.9 XPS spectra of 15CeNiNb C 1s. The peak at 284 eV is Carbon with the peaks ate 287 and 289.5 eV indicative of carbonate species.

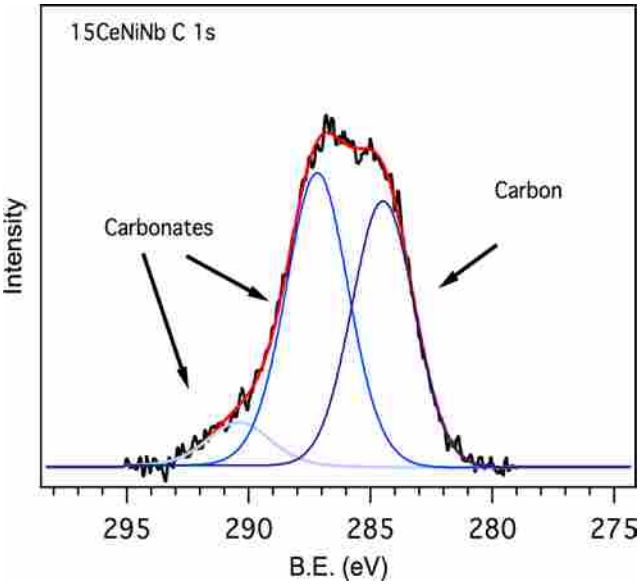

Table 3.5 Atomic percent of each element, binding energies, and species of 15CeNiNb.

	Ni 2p3/2	Ce 3d5/2			Nb 3p3/2		O1s
		A	B	C	A	B	A
At%.	32.27	1.63	0.29	1.75	0.73	0.81	62.52
BE	854	881.8	886.9	898.6	364.12	367.1	529-533.6

Table 3.6 Atomic percent of each element, binding energies, and species of 0.5CeNiNb.

0.5CeNiNb	Ni 2p3/2	Ce 3d5/2	Nb 3p3/2		O1s
		A	A	B	A
At%.	24.67	0.39	0.57	3.42	70.96
BE	854	881.8	360.7	365.5	524.7-530.3

Table 3.7 Atomic percent of each element, binding energies, and species of NiNb.

NiNb	Ni 2p3/2	Nb 3p3/2		O1s
		A	B	A
At%.	23.71	2.2	5.78	68.36
BE	853.6	361.6	364.4	526.4-530.9

Table 3.8 Ethylene production controls.

	350°C	
Catalyst	$X(C_2H_6)$	$S(C_2H_4)$
NiNb precipitate	36	57
0.5CeNiNb	39	57
2CeNiNb	30	55
4CeNiNb	37	50

References

1. Finiels, A.; Fajula, F.; Hulea, V., Nickel-based solid catalysts for ethylene oligomerization – a review. *Catal. Sci. Technol.* **2014,** *4*, 2412-2426.
2. Védrine, J., Heterogeneous Partial (amm)Oxidation and Oxidative Dehydrogenation Catalysis on Mixed Metal Oxides. *Catalysts* **2016,** *6*, 22.
3. Gärtner, C. A.; van Veen, A. C.; Lercher, J. A., Oxidative Dehydrogenation of Ethane: Common Principles and Mechanistic Aspects. *ChemCatChem* **2013,** *5*, 3196-3217.
4. Thorsteinson, E. M.; Wilson, T. P.; Young, F. G.; Kasai, P. H., The oxidative dehydrogenation of ethane over catalysts containing mixed oxides of molybdenum and vanadium. *J. Catal.* **1978,** *52*, 116-132.
5. Botella, P.; López Nieto, J. M.; Solsona, B.; Mifsud, A.; Márquez, F., The Preparation, Characterization, and Catalytic Behavior of MoVTeNbO Catalysts Prepared by Hydrothermal Synthesis. *J. Catal.* **2002,** *209*, 445-455.
6. Valente, J. S.; Armendáriz-Herrera, H.; Quintana-Solórzano, R.; del Ángel, P.; Nava, N.; Massó, A.; López Nieto, J. M., Chemical, Structural, and Morphological Changes of a MoVTeNb Catalyst during Oxidative Dehydrogenation of Ethane. *ACS Catal.* **2014,** *4*, 1292-1301.
7. Heracleous, E.; Lemonidou, A., Ni–Nb–O mixed oxides as highly active and selective catalysts for ethene production via ethane oxidative dehydrogenation. Part I: Characterization and catalytic performance. *J. Catal.* **2006,** *237*, 162-174.
8. Prior, T.; Giurco, D.; Mudd, G.; Mason, L.; Behrisch, J., Resource depletion, peak minerals and the implications for sustainable resource management. *Global Environmental Change* **2012,** *22*, 577-587.
9. Thota, S.; Kumar, J., Sol–gel synthesis and anomalous magnetic behaviour of NiO nanoparticles. *J. Phys. Chem. Solids* **2007,** *68*, 1951-1964.
10. Xia, Y.; Lin, M.; Ren, D.; Li, Y.; Hu, F.; Chen, W., Preparation of high surface area mesoporous nickel oxides and catalytic oxidation of toluene and formaldehyde. *J. Porous Mater.* **2016,** *24*, 621-629.
11. Nieto, J. M. L.; Solsona, B.; Grasselli, R. K.; Concepcion, P., Promoted NiO Catalysts for the Oxidative Dehydrogenation of Ethane. *Top. Catal.* **2014,** *57*, 1248-1255.

12. Skoufa, Z.; Heracleous, E.; Lemonidou, A. A., Unraveling the contribution of structural phases in Ni–Nb–O mixed oxides in ethane oxidative dehydrogenation. *Catal. Today* **2012,** *192*, 169-176.
13. Savova, B.; Loridant, S.; Filkova, D.; Millet, J. M. M., Ni–Nb–O catalysts for ethane oxidative dehydrogenation. *Appl. Catal., A* **2010,** *390*, 148-157.
14. Zhu, H.; Ould-Chikh, S.; Anjum, D. H.; Sun, M.; Biausque, G.; Basset, J.-M.; Caps, V., Nb effect in the nickel oxide-catalyzed low-temperature oxidative dehydrogenation of ethane. *J. Catal.* **2012,** *285*, 292-303.
15. Santander, J.; Lopez, E.; Diez, A.; Dennehy, M.; Pedernera, M.; Tonetto, G., Ni-Nb mixed oxides: One-pot synthesis and catalytic activity for oxidative dehydrogenation of ethane. *Chem. Eng. J.* **2014,** *255*, 185-194.
16. Zhu, H.; Dong, H.; Laveille, P.; Saih, Y.; Caps, V.; Basset, J.-M., Metal oxides modified NiO catalysts for oxidative dehydrogenation of ethane to ethylene. *Catal. Today* **2014,** *228*, 58-64.
17. Zhu, H.; Rosenfeld, D. C.; Harb, M.; Anjum, D. H.; Hedhili, M. N.; Ould-Chikh, S.; Basset, J.-M., Ni–M–O (M = Sn, Ti, W) Catalysts Prepared by a Dry Mixing Method for Oxidative Dehydrogenation of Ethane. *ACS Catal.* **2016,** *6*, 2852-2866.
18. Lin, X.; Xi, Y.; Sun, J., Unraveling the Reaction Mechanism for Nickel-Catalyzed Oxidative Dehydrogenation of Ethane by DFT: The C–H Bond Activation Step and Its Following Pathways. *J. Phys. Chem. C* **2012,** *116*, 3503-3516.
19. Lin, X. F.; Xi, Y. Y.; Phillips, D. L.; Guo, W. Y., The effect of a silica support: a density functional theory study of the C-H bond activation of ethane on a nickel oxide cluster. *J. Phys. Org. Chem.* **2016,** *29*, 134-144.
20. Varghese, J. J.; Mushrif, S. H., Insights into the C–H Bond Activation on NiO Surfaces: The Role of Nickel and Oxygen Vacancies and of Low Valent Dopants on the Reactivity and Energetics. *J. Phys. Chem. C* **2017,** *121*, 17969-17981.
21. Liu, Y.; Cong, P.; Doolen, R. D.; Guan, S.; Markov, V.; Woo, L.; Zeyß, S.; Dingerdissen, U., Discovery from combinatorial heterogeneous catalysis. *Appl. Catal., A* **2003,** *254*, 59-66.
22. Beckers, J.; Rothenberg, G., Sustainable selective oxidations using ceria-based materials. *Green Chem.* **2010,** *12*, 939.
23. Montini, T.; Melchionna, M.; Monai, M.; Fornasiero, P., Fundamentals and Catalytic Applications of CeO_2-Based Materials. *Chem. Rev.* **2016**, 116, 5987-6041.
24. Solsona, B.; Concepción, P.; Hernández, S.; Demicol, B.; Nieto, J. M. L., Oxidative dehydrogenation of ethane over NiO–CeO2 mixed oxides catalysts. *Catal. Today* **2012,** *180*, 51-58.
25. Huang, B.; Bartholomew, C. H.; Woodfield, B. F., Improved calculations of pore size distribution for relatively large, irregular slit-shaped mesopore structure. *Microporous Mesoporous Mater.* **2014,** *184*, 112-121.
26. Dietz, W. A., Response Factors for Gas Chromatographic Analyses. *J. Chromatogr. Sci.* **1967,** *5*, 68.
27. Zhu, H.; Rosenfeld, D. C.; Anjum, D. H.; Caps, V.; Basset, J. M., Green synthesis of Ni-Nb oxide catalysts for low-temperature oxidative dehydrogenation of ethane. *ChemSusChem* **2015,** *8*, 1254-63.

28. Heracleous, E.; Delimitis, A.; Nalbandian, L.; Lemonidou A.A.; HRTEM Characterization of the nanostructural features formed in highly active NiNbO catalysts for ethane ODH, *Appl. Catal., A* **2007**, 325, 220-226
29. Heracleous, E.; Lee, A.; Wilson, K.; Lemonidou, A., Investigation of Ni-based alumina-supported catalysts for the oxidative dehydrogenation of ethane to ethylene: structural characterization and reactivity studies. *Journal of Catalysis* **2005,** *231* (1), 159-171.
30. Brussino, P.; Bortolozzi, J. P.; Milt, V. G.; Banus, E. D.; Ulla, M. A., NiCe/gamma-Al2O3 coated onto cordierite monoliths applied to Oxidative Dehydrogenation of Ethane (ODE). *Catalysis Today* **2016,** *273*, 259-265.
31. Bêche, E.; Charvin, P.; Perarnau, D.; Abanades, S.; Flamant, G., Ce 3d XPS investigation of cerium oxides and mixed cerium oxide (CexTiyOz). *Surface and Interface Analysis* **2008,** *40* (3-4), 264-267.
32. Chagas, C. A.; de Souza, E. F.; Manfro, R. L.; Landi, S. M.; Souza, M. M. V. M.; Schmal, M., Copper as promoter of the NiO–CeO 2 catalyst in the preferential CO oxidation. *Applied Catalysis B: Environmental* **2016,** *182*, 257-265.
33. Crump, J. T. R. a. J. G., Crystallite Size Distributions of sintered Nickel Catalysts. *J. Catal.* **1979,** *57*, 417-425.
34. Kuo, H.K.; Ganesan, P.; DeAngelis, R.J.; The sintering of a Silica Supported Nickel Catalyst. *J. Catal.* **1980,** *64*, 303-319.
35. Liu, X.; Zhou, K.; Wang, L.; Wang, B; Li, Y.; Oxygen Vacancy Clusters Promoting Reducibility and Activity of Nanorods, *J. Am. Chem. Soc.*, **2009**, 131, 3140–3141.
36. Okolie, C.; Belhseine, Y. F.; Lyu, Y.; Yung, M. M.; Engelhard, M. H.; Kovarik, L.; Stavitski, E.; Sievers, C., Conversion of Methane into Methanol and Ethanol over Nickel Oxide on Ceria-Zirconia Catalysts in a Single Reactor. *Angewandte Chemie International Edition* **2017,** *56*, 13876-13881.
37. Hallac, B. B.; Brown, J. C.; Baxter, L. L.; Argyle, M. D., Structural and Functional Roles of Lanthana in Iron-Based High Temperature Water-Gas Shift Catalysts. *Int. J. Hydrogen Energy* **2014**, *39*, 7306-7317.

Chapter 4: Investigating the Unique Properties of Low wt% Ce Additive in NiNb Catalysts

Introduction

Recently it was observed that a very small amount of ceria in a CeNiNb ternary catalyst leads to the highest production of ethylene at temperatures as low as 300 °C.[1] When compared to a NiNb control prepared in the same manner, the ceria almost doubles the rate of ethylene production at that temperature. It was hypothesized that the major function of the Ce is to rapidly uptake and transfer oxygen to the active NiO sites. The rationale for observing higher activity at low wt% Ce was attributed to very small clusters of partially reduced CeO_2 that would be in direct contact with the NiO forming a Ni – O – Ce active center. However, the data from this study[1] was inconclusive and further analysis was necessary in order to identify the correct mechanism for the improved activity.

Ceria on its own is known for its redox activity[2] and is used as a combustion additive in catalytic converters to further oxidize CO to CO_2.[3] As a result, it is clear that as the concentration of CeO_2 increases the amount of combustion products in the ODH reaction should increase. This was confirmed by the increased conversion and decrease in selectivity of the 15%CeNiNb catalyst in the CeNiNb study. The observations reported by Solsona et.al.[4] for NiCe oxide catalysts give valuable insight into the interaction between the Ni and Ce. In their study NiCe catalysts were prepared using oxalic acid as a structuring agent to extend the surface area and pore structure of the catalyst. The high surface area and addition of Ce led to incremental increases in conversion at low temperatures as the amount of Ce was increased. The changes in activity and selectivity were partially attributed to the larger surface area and decreased size of the NiO crystallites but were also attributed to a synergistic effect of the Ni-Ce interaction. This

accurately describes what was observed in the CeNiNb report with high wt% Ce but does not account for the increase activity at low wt% Ce.

It is well known in the area of catalysis that adding even small amounts of a promoter can have drastic impacts on the catalytic activity.[5,6,7] In order to identify and accurately describe the impact of the small amount of Ce, more advanced techniques than used in the original characterization of the CeNiNb oxide catalyst needed to be considered. Since it is known that both NiO and CeO_2 have the potential to participate in the redox activity H_2-TPR was proposed as an easy experiment to assess if there are multiple redox sites in the catalysts. These redox sites would be observed as peaks at different temperatures indicating the reduction of oxygen at these sites.

The previous CeNiNb study showed that in any sample that contained less than 15wt% Ce, the CeO_2 phase was not observable by basic powder XRD. Synchrotron sources allow for much higher intensity of X-rays to be utilized[8] and thus can accurately analyze material that contain amorphous phases and crystallites with sizes smaller than 3 nm.[9] It was decided that EXAFS and XANES would give valuable insight. These techniques tell us what the oxidation state of each atom is, the number of atoms they are coordinated to, the bond lengths, and the local structure surrounding the atom being investigated. Since both Ce and Nb are unobservable in the CeNiNb samples this will provide crucial detail to the structure of the catalyst.

In this study, ternary CeNiNb oxide catalysts were prepared with $\leq$1% ceria oxide in order to identify the mechanism by which these low wt% materials facilitate such high reactivity. The catalysts are labeled x-CeNiNb where x is the wt% ceria. It is theorized that the Ce is facilitating a rapid uptake and transfer of oxygen to the NiO active sites facilitating higher redox activity. More in depth characterization was implemented in order to provide an understanding

of the structure and mechanism by which activity is increased. The outcomes of this study will facilitate improved catalyst performance for ODH of ethane.

Procedures for Catalyst Preparation

Catalyst preparation for CeNiNb oxide low wt% Ce: The NiNb oxide solid solution was prepared by adding 8 mmol nickel nitrate (Fisher Scientific certified grade) to 50mL of ethanol (Fisher Scientific) stirring at 400 rpm. After 3 minutes 1.2 mmol of niobium oxalate (Alfa Aesar) was added to the solution and stirred for another 5 minutes. At this point 9.2 mmol of oxalic acid (J.T. Baker) were added and stirred for 10 minutes at room temperature. The solution turned from a clear green to a milky green. The solutions were heated at 80°C for 30 minutes while stirring. The solution was then removed from the stir plate and dried in the oven at 100°C overnight. The solution was then ground in a mortar and pestle and put in a crucible for calcination. The oven was ramped at a rate of 3C/min to 400°C and held at 400°C for 4 hours.

The CeNiNb oxide solid solution was prepared on a slightly larger scale by mixing 16mmol nickel nitrate (Fisher Scientific certified grade) in 50mL of ethanol (Fisher Scientific)and stirring at 400 rpm for 2 min. Ceria nitrate at 0.186, 0.093, and 0.047 mmol (Alfa Aesar 99.5%) was added (to give 1,0.5,0.25%Ce) and stirred for another 3 minutes. Niobium oxalate (Alfa Aesar, 2.4 mmol) was added and stirred for 5 minutes. Then oxalic acid was acid was added in amounts that matched the total molar amount of the precursors 18.586, 18.493, 18.447 mmol oxalic acid for the 1, 0.5, 0.25% Ce respectively. The solution was stirred for 10 minutes and the solution turned from a clear green to a milky teal color. The solution was then heated at 80 °C for 30 minutes and the dried in an oven at 100 °C overnight. The solution was then ground in a mortar and pestle and put in a crucible for calcination. The oven was ramped at a rate of 3 °C/min to 400 °C and held at 400°C for 4 hours.

The characterization was done using the procedures explained in Chapter 2 for the following techniques or instruments: H_2-TPR, XRD, XPS, EXAFS, XANES and the flow reactor studies.

Data

H_2-TPR was used to observe the reducibility of the CeNiNb oxide catalysts to identify if multiple redox active sites exist. Nickel-niobium controls, (NiNb x where x is the method) were prepared by three different methods and then compared. (Figure 4.1) The different controls were used to show any difference in the redox potential in preparation method itself and the difference from pure NiO. The first method was the direct precipitation method involving only the nickel and niobium salt precursors.[10] The second was a precipitation method that included oxalic acid based on the method by Solsona et. al.[4] The third was a sol-gel preparation utilizing citric acid to form the gel.[11]

The $Ni_{0.85}Nb_{0.15}$ precipitate was the most reducible species with the reduction peak max at 308 °C and a shoulder centered around 398ºC. The high temperature shoulder has been attributed to the reduction of the Ni – O – Nb bond[10] which should have higher reduction potential than that of the Ni – O – Ni bond. This is a result of the Nb doping into the lattice of the NiO and binding the oxygen more tightly.

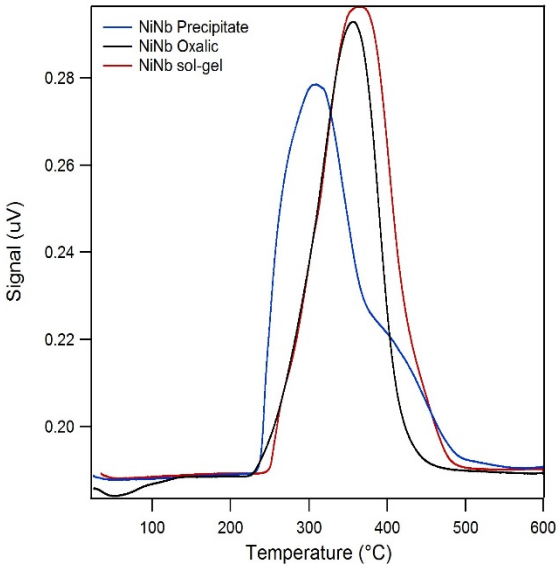

Figure 4.1 H2-TPR of NiNb prepared with different methods; precipitation (blue), oxalic acid addition (black), sol-gel formation (red).

The $Ni_{0.85}Nb_{0.15}$ sol-gel peak is centered at 364 °C. According to the Basset study, NiO shifts to higher and higher temperatures as the amount of Nb increases. As the Ni-Nb ratio increased the peak from Ni – O – Ni and Ni – O – Nb merge and only a single peak is observed representing the reduction of both species. The $Ni_{0.85}Nb_{0.15}$ oxalic peak is centered at 356 °C and the profile reflects that of the $Ni_{0.85}Nb_{0.15}$ sol-gel. This suggests that the redox activity of the $Ni_{0.85}Nb_{0.15}$ oxalic must be very similar the sol-gel catalysts and likely has formed an amorphous $NiNb_2O_6$ phase.

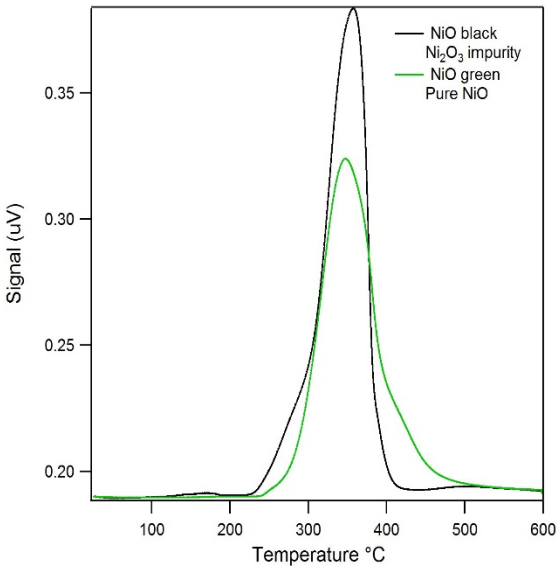

Figure 4.2 The comparison of "stoichiometric" (NiO green) and "non-stoichiometric" NiO (NiO Black).

H_2-TPR was performed on two commercial samples of NiO (Figure 4.2). One was green stoichiometric NiO and the other was a black nonstoichiometric NiO that has Ni_2O_3 impurities The shoulder at low temperature is the Ni_2O_3 impurity being reduced while the main peak is lattice NiO being reduced.[12] In comparison to the NiO samples in Figure 4.1, the NiNb precipitate matches the profile of the black NiO more than the green suggesting some Ni_2O_3 may remain in the sample. This is not ideal as this phase has been previously identified as the source of nonstoichiometric oxygen which leads to combustion products.[11]

In the H_2-TPR data of the samples that include a low wt% ceria (Figure 4.3), all of the profiles are very similar to the control NiNb. However, a small low-temperature shoulder appears around 254°C. The shoulder indicates that the redox activity of a small amount of the catalysts has been altered. This shoulder is present in both the 0.25 and 0.5 wt% Ce samples but is slightly larger in the 0.25%CeNiNb. The 0.25%CeNiNb proves to be the most active catalyst in this series and must be tied to this small change in redox activity.

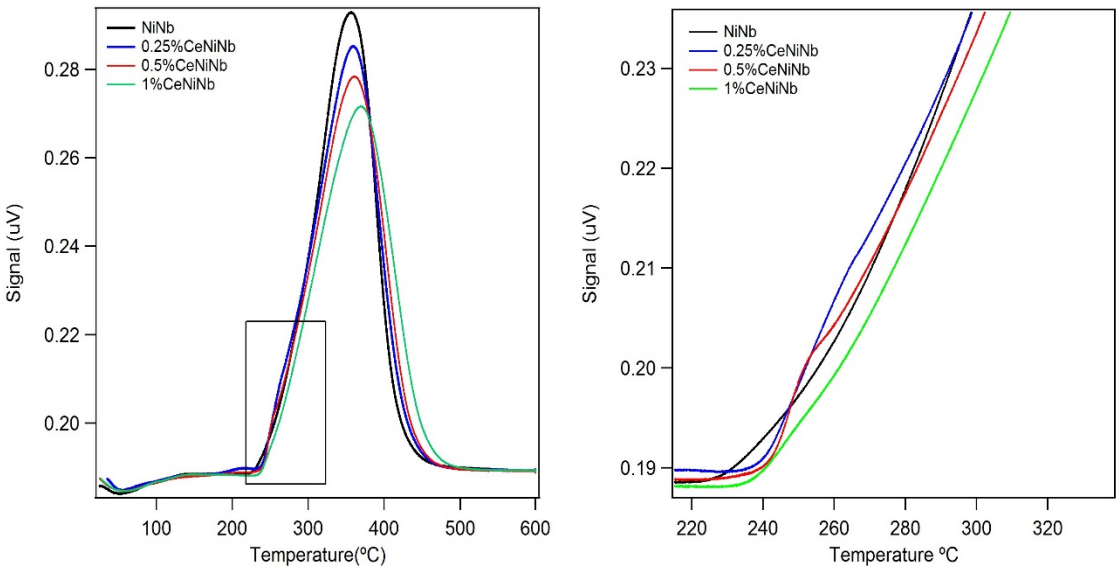

Figure 4.3 H_2-TPR of low wt% ceria catalysts prepared by the oxalic method where the wt% refers to the wt% of Ce with a set Nb-Ni ratio of 0.176; NiNb control (black), 0.25wt% CeNiNb (blue), 0.5wt% CeNiNb (red), 1.0wt%CeNiNb (green). The Square in the left image is expanded on the right.

The H_2-TPR data shows that the redox potential for the 0.25%CeNiNb catalyst has been altered but doesn't tell us anything about how that might have happened. Powder X-ray diffraction was performed on the low weight percent ceria-nickel-niobium oxide catalysts (Figure 4.4) The 0.25-1CeNiNb catalysts all showed similar diffraction patterns to that of the $Ni_{0.85}Nb_{0.15}$ control. As in the previous study this shows that the ceria is unobservable by powder XRD. The broad peak from ~22-35 2θ has been attributed to amorphous niobium.[13] The nickel however, is easily observed[14] with peaks at 37, 43, 62, 75, 79, 95, 106, 111 2θ and exhibits crystallite sizes of 7-8 nm for all samples.

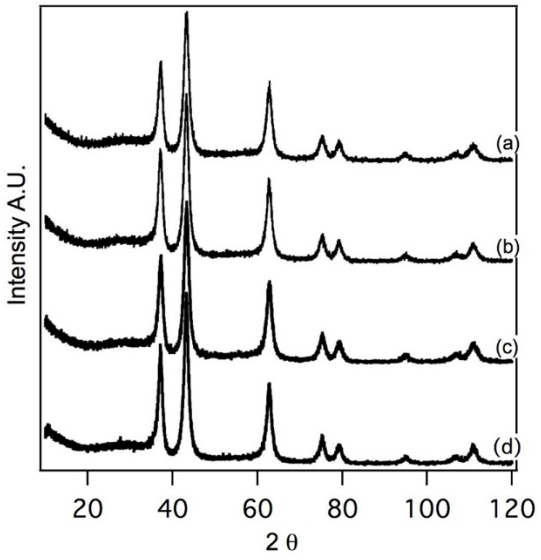

Figure 4.4 Powder X-ray diffraction patterns for CeNiNbOx catalysts (a)1%CeNiNb, (b) 0.5%CeNiNb, (c) 0.25% CeNiNb, (d) Ni0.85Nb0.15.

Rietveld refinement was performed in order to assess any changes in the lattice parameters as this gives insight into how well a heteroatom has doped into the lattice or if an amorphous phase has developed. Pure NiO has a lattice parameter of 4.176.[14] In these samples it is clear that the lattice parameters have gotten much larger (Table 4.1). In the precipitate method the doping of the niobium caused a reduction of the lattice constant. In the sol-gel prep the lattice constant also increased and was attributed to the formation the amorphous Ni-Nb phase. This is likely what happens in the CeNiNb oxide since Ce is too large of an atom to reasonably dope into the NiO lattice.

Table 4.1 Lattice parameters obtained through Rietveld refinement using PANalytical Xpert Pro software.

Catalyst	NiO Lattice constant (Å)
$Ni_{0.85}Nb_{0.15}$ Oxalic	4.1809
0.25% CeNiNb	4.1813
0.5%CeNiNb	4.1816
1%CeNiNb	4.1819

XRD analysis doesn't show any indication that the Ce is present in the catalyst. XPS was used to ensure that the Ce was in the samples. However, another main reason for using XPS is to obtain information regarding the oxidation states of the metals. XPS analysis was performed on each of the samples and is surface sensitive. As a result the composition at the surface may not reflect that of the expected composition of the entire material. The composition of each catalyst's surface was derived from the integration of the Ce 3d, Ni 2p, Nb 3p, and the O 1s core emission spectra (Table 4.2). The ratio of ceria to nickel at the surface is much higher than the amount of ceria that was added by impregnation. This suggests that almost all the Ce that was added to the catalysts migrates to the surface of the catalyst during the initial calcination. There also seems to be a minor trend of the Nb being forced into the bulk of the material with increasing amounts of Ce shown by the decreasing amount of Nb. This trend for Nb however, may just be an artifact of the larger amounts of Ce at the surface blocking the observed Nb.

Table 4.2 The surface composition of the metals in the catalysts as recorded from the peak fitting of XPS analysis.

	Surface composition (%)			
	Ni	Nb	Ce	O
1% Ce	33.83	4.26	2.47	59.45
0.5% Ce	33.79	4.43	2.25	59.54
0.25% Ce	32.25	5.12	2.80	60.43
NiNb	33.04	5.40	0.00	61.56

Up to this point in the study the impact the ceria is having on the catalyst is still unclear. It alters the redox properties and is mostly all on the surface, but requires further characterization in order to obtain an understanding of how it is changing the redox properties of the catalyst. In order to understand the local environment of the Ce, the NiNb oxalic, 1%CeNiNb, and the 0.25%CeNiNb samples were taken to the synchrotron radiation source at Brookhaven National

Lab (BNL) and then later to Argonne National Lab. The samples were analyzed on the QAS beamline at Brookhaven and beamline 20 at Argonne. The 1% and 0.25% Ce samples were chosen to show the contrast in a sample with high activity vs. marginal activity. Only the nickel and niobium were observable using the 30 scans that were taken at BNL. In order to try to completely identify the ceria in the samples they were analyzed again on beamline 20 at the advanced photon source (APS).

NiO and nickel metal were used as standards for the nickel analysis, Nb_2O_5 and NbO_2 were used for the niobium analysis controls, and then CeO_2 and cerium nitrate hexahydrate were used for ceria analysis controls. The XANES data was very clear for all three samples. The nickel K edge of each of the NiNbCe samples is almost identical to the NiO standard indicating that all of the nickel oxide is in the Ni^{2+} oxidation state. In the data for the niobium K edge the two controls show Nb^{4+} for NbO_2 and Nb^{5+} for Nb_2O_5. All the samples directly resemble the Nb_2O_5 showing that it is the dominant phase in all of the catalysts prepared by the oxalic method.

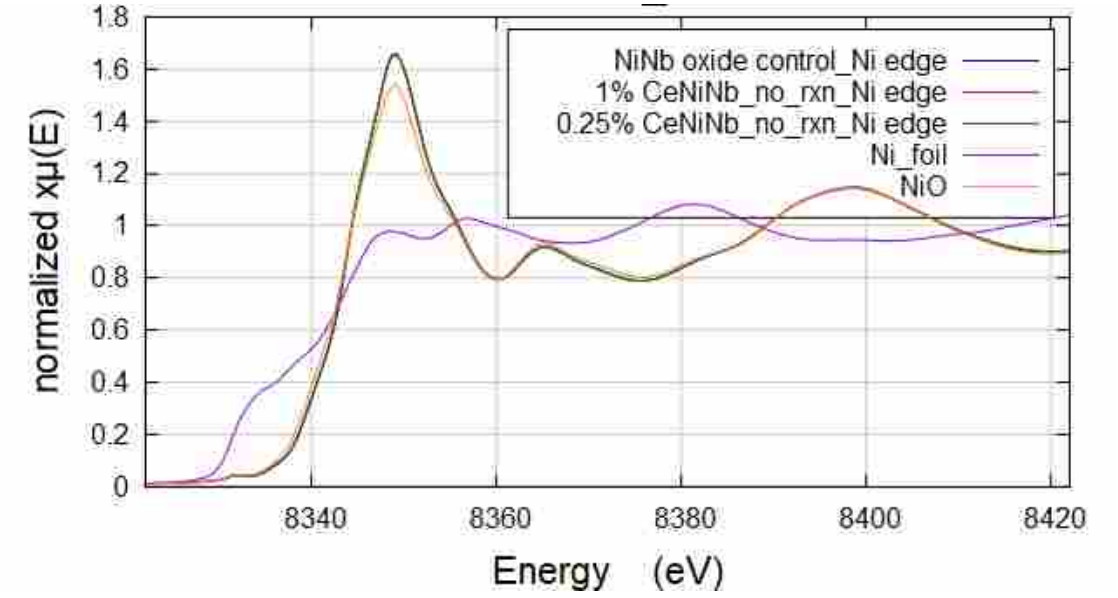

Nickel K edge

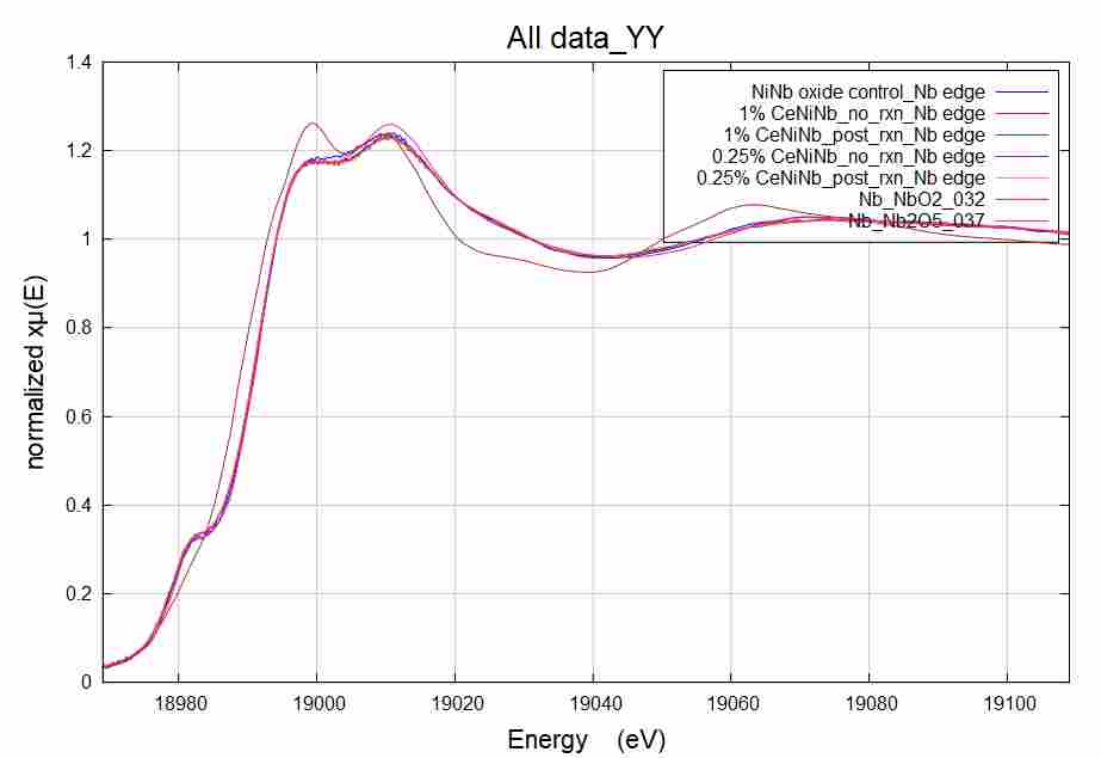

Niobium K edge

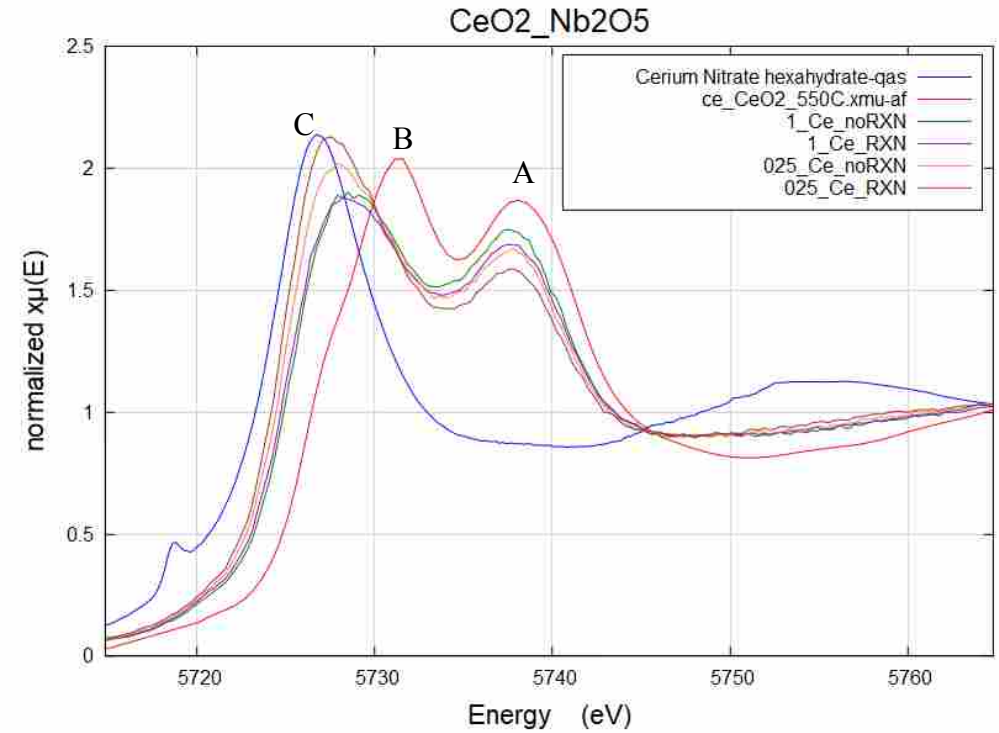

Ceria L_{III} edge

Figure 4.5 XANES data for the Ni K edge NiO and samples vs. Ni metal, B Nb K edge showing the similarity between samples and Nb_2O_5 vs. NbO2, and C Ce LIII edge showing the difference between the CeO_2 and the $Ce(NO_3)_3*6H_2O$ with the 1 and 0.25% pre vs. post reaction.

In the ceria L_{III} edge data, two controls were analyzed: cerium nitrate for Ce^{3+}, and cerium nitrate that had been calcined at 550°C for CeO_2 or Ce^{4+}. All four samples analyzed have a doublet that doesn't exactly match up with doublet of the CeO_2 at 5737eV and 5731eV (Peak A and B respectively). However they have a similar peak shape suggesting a large majority of the ceria is in the Ce^{4+} oxidation state but that the Ce^{3+} (Peak C 5726eV) is also present. There doesn't appear to be much of a difference between the pre- and post- reaction samples for the 1%CeNiNb catalyst. This would suggest that as the reaction proceeds it is not significantly reduced.

The data for the pre- and post- reaction 0.25%CeNiNb is very different from that of the 1% catalysts. In the 0.25%CeNiNb the pre-reaction catalysts starts with a larger initial concentration of Ce^{3+}. When it is compared to the post-reaction sample, the lower energy peak shifts very slightly to lower energy. This shows that not only does the 0.25%CeNiNb catalyst start with more Ce^{3+} content but that the number of Ce^{3+} species increases as the reaction proceeds. This suggests that the Ce^{3+} participates in the reaction and must be a key part of the mechanism facilitating the increased activity of this catalyst.

The XANES data gives a very clear picture of the oxidation states of all the metal oxides while the EXAFS data outlines the local environments of those atoms. The EXAFS data that was analyzed confirms the XANES data for the nickel and niobium species showing that NiO is present for the nickel phase and Nb_2O_5 for the niobium. The ceria EXAFS data is used to identify if there is a heteroatom in the 2nd coordination shell of the ceria. There are two distinctive peaks

in the R-space to consider the one at approximately 1.8 Å and the one at 2.4 Å. These give information regarding the first and second neighbors of the Ce atom. The one at approximately 1.8 Å is the contribution of Ce-O. As can be seen in the data this peak shifts to shorter distances for the 1%CeNiNb and even shorter for the 0.25%CeNiNb catalysts. This is indicative of a more strongly bound oxygen bond.

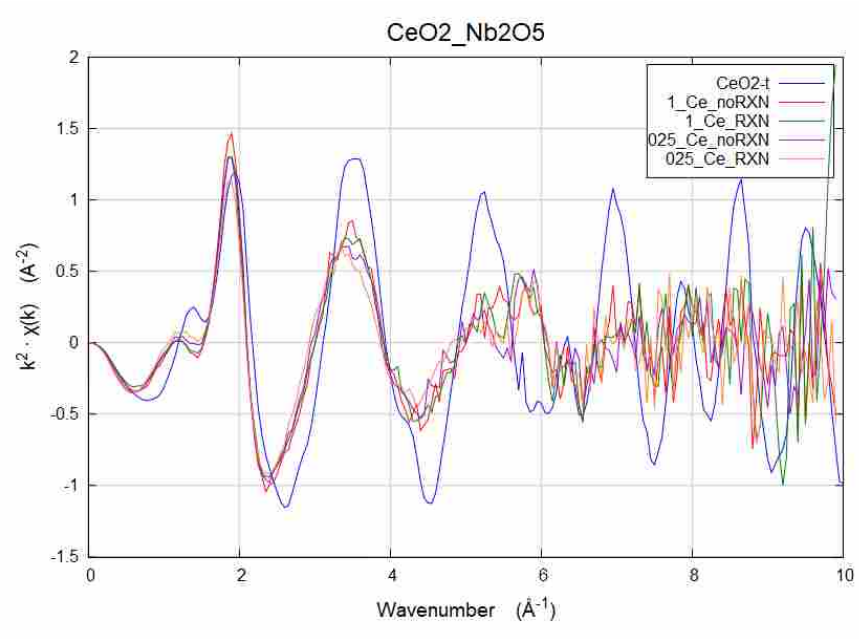

Ce k space

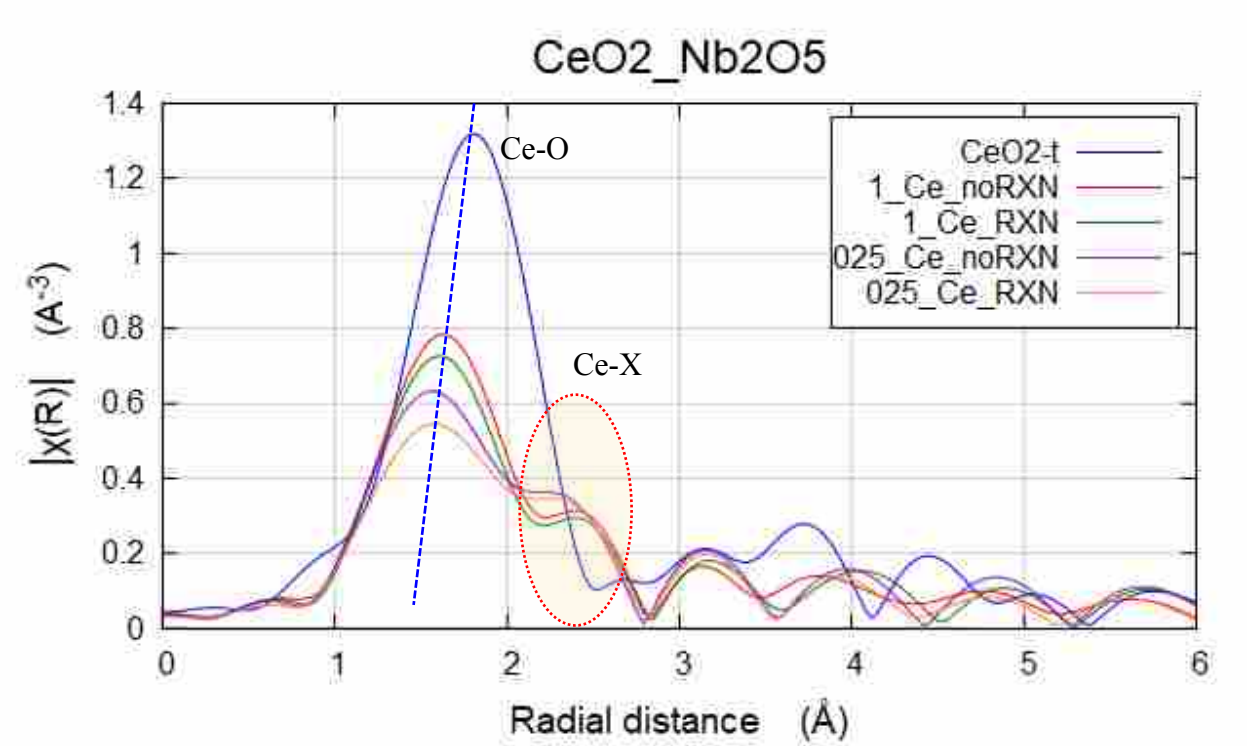

Ce R-space

Figure 4.6 EXAFS data for Ce LIII edge showing k space and R-Space for CeO_2 control, 1% and 0.25%Ce pre and post reaction samples.

When the catalyst samples are compared with the control it is clear that the peak at 2.4 Å is not present in the control. In the control, peaks related to the Ce-Ce interaction do not occur until 3-4 Å.[15] This suggests that the peak at 2.4 Å must be the interaction of Ce with a heteroatom. Unfortunately it is not clear from the EXAFS data what atom this actually represents, as it could be Ni or it could be Nb. For the 1% sample, the intensity of Ce-O peak decreases and the Ce-X peak increases a little bit. This is a reflection of the concentration of the Ce-O bond decreasing the concentration of the C-X interaction increasing. In the 0.25% sample, the same trend is observed but both the Ce-O and the Ce-X interaction shift to shorter lengths. These changes suggest differences in the coordination numbers, bond distances, and disorders of

Ce-O and Ce-X in 1% and 0.25% samples. This change is more significant for Ce-O peak and could be due to the decrease of the coordination number or the increase of the disorder factor.

With a better understanding of how the metal oxides are interacting in the catalysts the catalysts were tested in a custom-built flow reactor in the temperature ranges of 200-400°C and a total flow rate of 10mL/min. The ratio of ethane to oxygen was kept at a 1:1 ratio for a total of 2 mL of the flow. For all of the samples there was no conversion observed at 200°C.

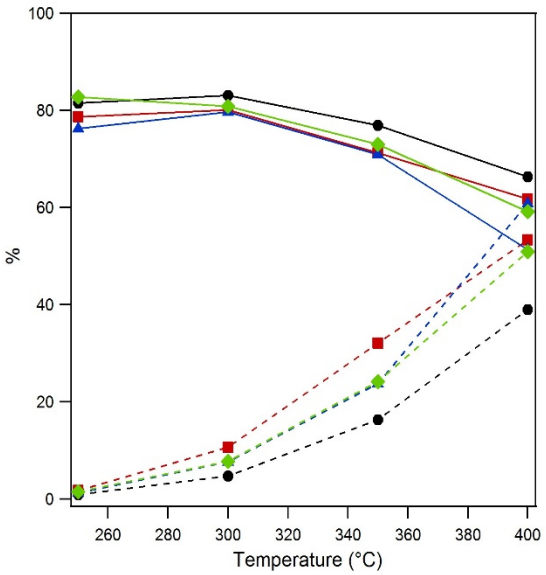

Figure 4.7 C2H6 conversion (dotted line) and C_2H_4 selectivity (solid line). Black Ni0.85Nb0.15, Red 0.25%CeNiNb, Blue 0.5%CeNiNb, Green 1%CeNiNb.

The 0.25% CeNiNb is the most active of all the Ce containing catalysts. This is in agreement with our previous study in which our lowest wt% Ce catalyst also outperformed the catalysts with higher loadings of Ce. The selectivity of the catalysts' with the Ce additive are only slightly lower than that of the NiNb catalyst (Figure 4.7). However, the conversions have improved dramatically. This is most significant at 350 °C. The large increases in the conversion while maintaining high selectivity lead to dramatic improvements in the overall yields of ethylene.

Discussion

Based on the analysis of the low wt% Ce catalysts thus far, it is clear that ceria plays a key role in altering the mechanism of the reaction leading to a higher production of ethylene. This is especially true in the 0.25%CeNiNb catalyst. The H_2-TPR data shows that the addition of the Ce introduces a small shoulder in the reduction profile of the 0.25 and 0.5%Ce catalysts showing a new redox site in the catalysts. Based on the XPS analysis most of the Ce appears to be on the surface of the catalysts and indicates that the ceria is likely performing as theorized by rapidly adsorbing oxygen from the feed.

The 0.25%CeNiNb facilitates the highest rates of ethylene production and differs from the 1%CeNiNb catalyst in all the characterization. The EXAFS and XANES data for the comparison of the 1% vs 0.25% Ce samples, or the marginally active catalysts compared to the highly active catalyst, opens up a couple of new theories on the possible mechanism. First in the XANES data for the ceria the amount of Ce^{3+} increases in the pre- and post- reaction samples. This increase suggests that the ceria is participating in the redox cycle. Second, the shoulder at 2.4 Å in the R-space of the EXAFS shows that there is a Ce-X interaction. The resolution doesn't allow the specifics of the exact Ce-X interaction to be identified, however, based on the catalyst composition this could be a Ce – O – Ni or a Ce – O – Nb bond. The distance between O and the unknown atom is ~0.7 Å. Both the Ni – O and Nb – O bond length for NiO and Nb_2O_5 are that same distance making it unclear which is actually present.[16] Based on the redox properties and activity increases, it is more likely that it is the Ce – O – Nb bond. Ceria is reduced as the reaction proceeds, which indicates that a higher valence species is facilitating the reduction.[17] Initially Nb was introduced into the catalyst to alter the redox properties except it was initially only to keep Ni in the 2+ oxidation state. Also, a Ce – O – Ni interaction would likely decrease

the activity of the catalyst since the oxygen in this linkage would be more tightly bound than the Ni – O – Ni bond known for this reaction. This more tightly bound oxygen would be less active for the reaction.

Since it is still fairly unclear which atom the Ce-X path in the R-Space indicates further studies are necessary to solidify the mechanism for the increased activity. The easiest and most direct experiment that remains is to prepare a CeNb oxide catalyst with similar ratios to that seen on the surface of the 0.25%CeNiNb catalyst and test it under the same conditions used for the oxidative dehydrogenation using the CeNiNb catalyst. If our theory is correct the new catalyst should exhibit both higher conversions and higher selectivity than the pure Nb_2O_5. The higher conversion would show that the catalyst has a redox center whereas the Nb_2O_5 is not active. The higher selectivity would show that the oxygens at the surface are changed from the electrophilic oxygens leading to combustion to less active oxygens leading to the ethylene.

References

1. Park, J. L.; Balijepalli, S. K.; Argyle, M. D.; Stowers, K. J., Low Temperature Oxidative Dehydrogenation of Ethane by Ce-Modified NiNb Catalysts. *Industrial & Engineering Chemistry Research* **2018,** *57* (15), 5234-5240.
2. Beckers, J.; Rothenberg, G., Sustainable selective oxidations using ceria-based materials. *Green Chemistry* **2010,** *12* (6), 939-948.
3. El Fallah, J.; Boujana, S.; Dexpert, H.; Kiennemann, A.; Majerus, J.; Touret, O.; Villain, F.; Le Normand, F., Redox Processes on Pure Ceria and on Rh/CeO2 Catalyst Monitored by X-Ray Absorption (Fast Acquisition Mode). *The Journal of Physical Chemistry* **1994,** *98* (21), 5522-5533.
4. Solsona, B.; Concepcion, P.; Hernández, S.; Demicol, B.; Nieto, J. M., *Oxidative dehydrogenation of ethane over NiO–CeO 2 mixed oxides catalysts*. **2012**; Vol. 180.
5. Thorsteinson, E. M.; Wilson, T. P.; Young, F. G.; Kasai, P. H., The oxidative dehydrogenation of ethane over catalysts containing mixed oxides of molybdenum and vanadium. *Journal of Catalysis* **1978,** *52* (1), 116-132.
6. Sarkany, A.; Zsoldos, Z.; Stefler, G.; Hightower, J. W.; Guczi, L., Promoter Effect of Pd in Hydrogenation of 1,3-Butadiene over Co-Pd Catalysts. *Journal of Catalysis* **1995,** *157* (1), 179-189.
7. Ueda, W.; Oshihara, K., Selective oxidation of light alkanes over hydrothermally synthesized Mo-V-M-O (M=Al, Ga, Bi, Sb, and Te) oxide catalysts. *Applied Catalysis A: General* **2000,** *200* (1), 135-143.

8. Kunz, C., Meeting of Technology arising from High-energy Physics, v.1, CERN, Geneva, Switzerland, 24-26 Apr 1974, pp. 155-66.
9. Newville, M., Fundamentals of XAFS. *Reviews in Mineralogy and Geochemistry* **2014,** *78* (1), 33-74.
10. Heracleous, E.; Lemonidou, A., Ni–Nb–O mixed oxides as highly active and selective catalysts for ethene production via ethane oxidative dehydrogenation. Part I: Characterization and catalytic performance. *Journal of Catalysis* **2006,** *237* (1), 162-174.
11. Zhu, H.; Ould-Chikh, S.; Anjum, D. H.; Sun, M.; Biausque, G.; Basset, J.-M.; Caps, V., Nb effect in the nickel oxide-catalyzed low-temperature oxidative dehydrogenation of ethane. *Journal of Catalysis* **2012,** *285* (1), 292-303.
12. Mile, B.; Stirling, D.; Zammitt, M. A.; Lovell, A.; Webb, M., The location of nickel oxide and nickel in silica-supported catalysts: Two forms of "NiO" and the assignment of temperature-programmed reduction profiles. *Journal of Catalysis* **1988,** *114* (2), 217-229.
13. Heracleous, E.; Delimitis, A.; Nalbandian, L.; Lemonidou, A. A., HRTEM characterization of the nanostructural features formed in highly active Ni–Nb–O catalysts for ethane ODH. *Applied Catalysis A: General* **2007,** *325* (2), 220-226.
14. K. Martin and G. McCarthy: North Dakota State Univ., Fargo, ND, USA, ICDD Grant-in-Aid (1991).
15. Clark, A. H.; Marchbank, H. R.; Hyde, T. I.; Playford, H. Y.; Tucker, M. G.; Sankar, G., Reverse Monte Carlo studies of CeO2using neutron and synchrotron radiation techniques. Physica Scripta **2017**, 92 (3), 034002.
16. Shannon, R., Revised effective ionic radii and systematic studies of interatomic distances in halides and chalcogenides. *Acta Crystallographica Section A* **1976,** *32* (5), 751-767.
17. Heracleous, E.; Lemonidou, A., Ni–Nb–O mixed oxides as highly active and selective catalysts for ethene production via ethane oxidative dehydrogenation. Part I: Characterization and catalytic performance. *Journal of Catalysis* **2006,** *237* (1), 162-174.

Chapter 5: Supplementary Info for Identifying the Structural and Electronic Properties of Mixed Metal Oxides for Ethane ODH

Introduction

Recently it has become clear that the electronic effects of introducing niobium as an additive in the catalyst is not singular to niobium.[1-4] The ability of the Nb to dope into the cationic vacancies[4] of the NiO and facilitate a reduction of the Ni^{3+} to Ni^{2+} can be performed by any higher valence additive.[5] Similar amounts of titanium, tungsten, and tin additives were combined with a nickel catalyst in a novel preparation involving grinding in order to compare to the activity of niobium additives. The method produced catalysts with higher low temperature productivity to ethylene than had been observed with niobium additives.[5] This outcome is due to the fact that not only the additive has an effect on the productivity but also the preparation method which enhances the active sites by decreasing the crystallite size and increasing the surface area.

The oxalic method used in the preparation of the CeNiNb catalysts has not been utilized in many other studies. As such, it is important to validate some of the findings proposed for other preparations to see if they hold true for the precipitation method using oxalic acid. A few studies were performed in order to identify the properties of different metal oxide additives using the same preparation technique used in the CeNiNb catalyst.

In this study, three different types of catalysts were prepared. A series of NiTi oxide catalysts were made to test the effects of the metal in comparison to the niobium. Ti has already been shown in the grinding method to be a suitable replacement for niobium. We wanted to show this held true for the oxalic preparation but also to test if Ti exhibited the similar uptake and transfer properties for oxygen known for the Ce additive.

Next a series of NiCe oxide catalysts were prepared to investigate the performance of Ce without the benefit of niobium. The CeNiNb catalyst has unique redox properties and it is unclear whether this stems from an interaction with the Ni or the Nb. The work of Solsona et. al.[6] had previously shown that the productivity increases with increasing amount of ceria in the NiCe so the activity of the CeNiNb was unusual. Their study was repeated with some minor changes that reflect similar prep to the CeNiNb in order to verify the reactivity and see if the unique redox activity was seen in the NiCe.

The third study included the preparation of a series of NiTiCe oxide catalysts. The purpose of this study was to see if the Ce affects the NiTi in the same way as the NiNb and to see how it compares with the CeNiNb catalyst for the ODH of ethane. It was hypothesized that the reaction would be very similar and therefore it was assumed that the Ti might also contribute to the uptake and transfer of oxygen.

All of the catalysts in the three studies were prepared with only the basic characterization of these catalysts performed. This included N_2 adsorption studies to isolate the surface areas, pore volumes, and pore size. The phase of each oxide present and the crystallite size of each of the species were identified using powder XRD. After characterization the catalysts were tested in the custom-built flow reactor for activity of oxidative dehydrogenation of ethane. Reaction conditions were similar to those used in the CeNiNb study with flow rates of 10 ml/min total flow with a 1:1 ratio of ethane to oxygen excess N_2 and tested from 200-400°C. Procedures for the preparation of NiTi, NiCe and NiTiCe oxide catalysts are in the experimental section.

Procedures for Catalyst Preparation

NiTi oxide: The NiTi oxide catalysts were prepared by dissolving 16 mmol nickel nitrate (Alfa Aesar) in 50 mL of ethanol (Fisher) stirring at room temperature. After 3 minutes titania

isopropoxide (Sigma-aldrich) was added to get 5, 10, 15, 20 % titania. The solution was stirred for 2 minutes before oxalic acid (JT Baker) that matched the total molar value of the metal precursors was added to the solution and stirred for another 10 minutes. It formed a milky precipitate and was transferred to a stir plate and heated at 80°C for 30 minutes to evaporate the ethanol. The solution was then dried out overnight at 110°C. The catalysts were calcined in a muffle furnace by ramping at 3°C/min from room temperature to 400°C and then holding at 400°C for 4 hours.

NiCe oxide: NiCe oxide catalysts were prepared by dissolving 16 mmol nickel nitrate (Alf Aesar) in 50 mL of ethanol (Fisher) stirring at room temperature. After 3 minutes ceria nitrate (Alfa Aesar) was added to get 1, 5, 10, 15, 25, and 50% ceria. The solution was stirred for 3 minutes before oxalic acid (JT Baker) that matched the total molar value of the metal precursors was added to the solution and stirred for another 10 minutes. It formed a milky precipitate and was transferred to a stir plate and heated at 80°C for 30 minutes to evaporate the ethanol. The solution was then dried out overnight at 110°C. The catalysts were calcined in a muffle furnace by ramping at 3°C/min from room temperature to 400°C and then holding at 400°C for 4 hours

NiTiCe oxide: In the NiTiCe oxide catalysts, the nickel and titania were kept at a constant molar ratio of 0.25 Ti:Ni The catalyst were prepared by dissolving 16 mmol nickel nitrate (Alfa Aesar) in 50 mL of ethanol (Fisher) stirring at room temperature. After 3 minutes 4 mmol titania isopropoxide (Sigma-aldrich) was added and stirred for 3 minutes. Then ceria nitrate (Alfa Aesar) was added to get 1, 5, and 20wt% ceria. The solution was stirred for 5 minutes before oxalic acid (JT Baker) that matched the total molar value of the metal precursors was added to the solution and stirred for another 10 minutes. It formed a milky precipitate and was transferred

to a stir plate and heated at 80°C for 30 minutes to evaporate the ethanol. The solution was then dried out overnight at 110°C. The catalysts were calcined in a muffle furnace by ramping at 3°C/min from room temperature to 400°C and then holding at 400°C for 4 hours.

Characterization: All characterization was completed according the procedures outlined in chapter 2 for powder XRD, N_2-adsorption, and the flow reactor experiments.

Data

In the first study involving the NiTi catalysts, titania was added at 5, 10, 15, and 20 wt% which are the same ratios that were used in the grinding method. Among these samples the only peak observed for titania is a very broad peak at 23° 2θ (Figure 5.1). As the amount of titania increases this peak gets more defined as would be expected from the crystallite sizes getting larger. All other peaks represent the NiO phase.[8]

The crystallite properties and the surface properties for the entire series of NiTi catalysts are compared in Table 5.1. According to the analysis of the size via the Scherer equations the NiO crystallites gradually decrease as the concentration of Ti increases. This same trend was observed in the grinding method but has much larger variance ranging from 12 nm down to 4 nm in their 20wt%Ti sample. The decreasing size shows that the TiO_2 phase is inhibiting the aggregation of the NiO. The lattice constant of the NiO doesn't change significantly but does gradually increase with increasing Ti content. The fact that the lattice constant doesn't decrease suggests that it is not likely that much of the Ti doped into the NiO lattice. An amorphous Ni-Ti phase seems to have formed similar to the amorphous phases of NiNb prepared in the same manner.

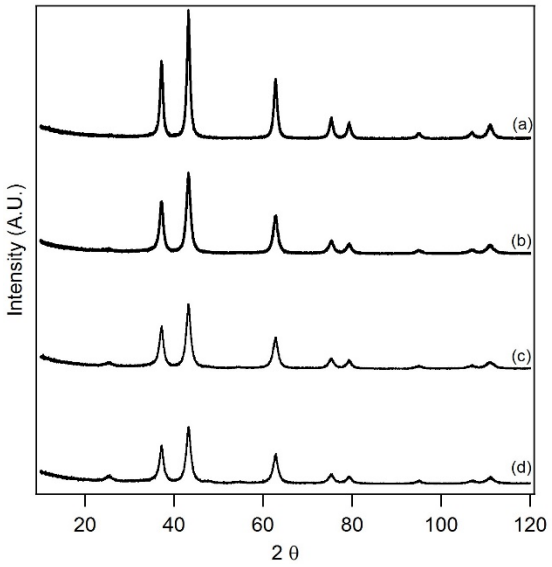

Figure 5.1 Powder diffraction data for the series of NiTi catalysts (a) 5% NiTi, (b) 10% NiTi (c) 15% NiTi, (d) 20% NiTi.

After the phases were analyzed by XRD the surface properties of the NiTi catalyst were analyzed by N_2 adsorption. The N_2 adsorption data shows that with low loadings of titania the surface area of the catalyst is very low. As the amount of Ti increases the surface areas and pore volumes also increase. This suggests that at higher Ti concentrations an extended amorphous Ni-Ti oxide phase forms with an expanded pore structure. The increasing NiO lattice constant for these catalysts also supports this idea.

Table 5.1 N_2 adsorption data for nickel-titania catalysts.

Cataylst	**NiO Crystallite Size (nm)**	**NiO Lattice constant (Å)**	**TiO_2 Crystallite Size (nm)**	**BET Surface Area (m^2/g)**	**Pore Volume (cm^3/g)**	**Pore Size (Å)**
NiNb		4.1808		142.65	0.54	116.85
5%Ti NiTi	8.2	4.1804	<0.5	75.51	0.48	116.85
10%Ti NiTi	7.0	4.1803	0.5	107.62	0.57	167.57
15%Ti NiTi	6.7	4.1813	0.9	171.13	0.88	163.59
20%Ti NiTi	6.5	4.1815	3.3	199.54	1.02	159.37

Even with just two simple characterizations it is enough to see that some of the properties of the catalysts are similar to the grinding method, but some of them are similar to the NiNb prepared by the oxalic preparation. The samples were tested in the flow reactor using the conditions described in Chapter 2. The flow reactor data for the NiTi catalysts show high selectivities for all the catalysts except the 5wt%Ti sample (Figure 5.2). The selectivity of 5wt%Ti is higher than pure NiO showing that the Ti additive is beginning to change the electronics of the electrophilic oxygens in the NiO. However, since the XRD shows that not very much of the Ti dopes into the lattice, the Ni vacancies do not seem to be filled until higher concentrations of Ti are reached.

As the amount of titania increases the selectivity for ethylene at 250°C gets as high as 80%. However, the 15 wt% NiTi sample seems to have the most stable selectivity as the conversion and temperature increase. The 20wt% NiTi overall has the highest selectivity and highest conversion. This was true for the grinding method as well. This performance is not significantly different from that of the 10 and 15wt% NiTi, so it is likely that it is only the smaller size and increased surface area that account for the differences in these catalysts. However, the overall performance of these catalysts is directly related to the amount of Ti that has doped into the NiO cationic vacancies. This binds the nonstoichiometric oxygen more tightly and reduces the Ni^{3+} to Ni^{2+} which is exactly the same effect enabled by using the niobium additive.

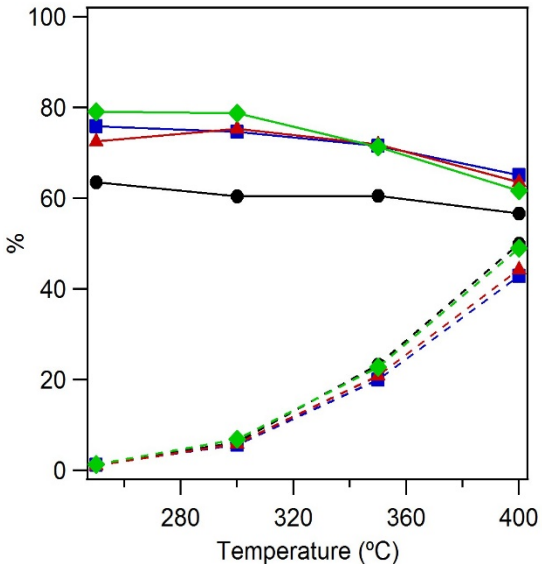

Figure 5.2 Solid lines are selectivity, dotted lines are conversion. Black (5wt% NiTi), Red (10wt% NiTi) Blue (15wt% NiTi), Green (20wt% NiTi).

In order to clarify the role of ceria in the CeNiNb catalysts, and to confirm Solsona's results, a series of 1-50 wt% ceria in nickel catalysts were prepared. The catalysts were first characterized by powder XRD and the results are shown in the diffraction patterns in Figure 5.3. At 1wt% Ce there is no observable peak for ceria. However, at 5wt% Ce and above it is clear that a CeO_2 phase is present in the catalyst. As the loading of ceria increases the size of the NiO crystallite is inhibited. At 50wt% Ce the growth of the NiO crystallite is so inhibited that the peaks for NiO are almost unobservable.

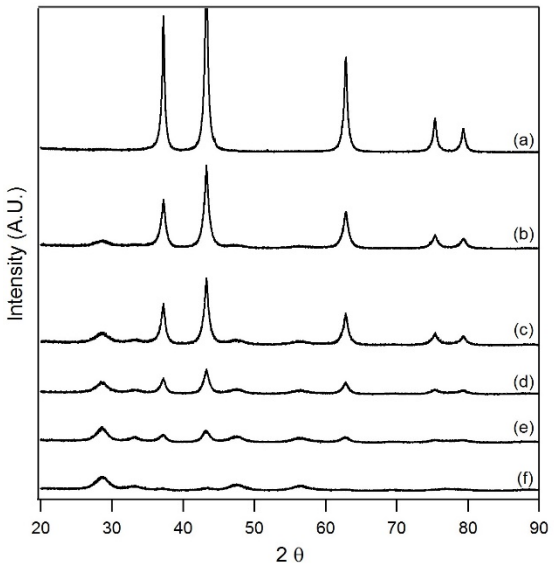

Figure 5.3 X-ray diffraction patterns for the series of Ni-Ce oxide catalysts. (a) 1%NiCe, (b) 5%NiCe, (c) 10%NiCe, (d) 15%NiCe, (e) 25%NiCe (f) 50%NiCe.

The sizes for both the NiO and CeO_2 phase are analyzed using the Scherer equation for the 1-50wt% NiCe catalysts. The size of the NiO decreases sharply from the 1-5wt%Ce samples. The size then increases followed by a drastic decrease again from 15-25wt%Ce samples. The changes in the size of the NiO are mainly due to the aggregation of the NiO being inhibited by the CeO_2 phase and then later the drastic change from 15-25% is likely due to incorporation of the NiO into the CeO_2 lattice.

The lattice parameters for both the NiO and CeO_2 were calculated. The NiO lattice parameter gradually increases and the CeO_2 gradually decreases as the wt% of Ce increases. This indicates that there is a strong interaction between the nickel and ceria. The increasing lattice parameters of the NiO are a good indication of the formation of an amorphous Ni-Ce phase. Whereas the decreases in the lattice parameters for the CeO_2 also indicate the formation of the amorphous layer, they may also suggest that the Ni is doping in the lattice of the CeO_2. This is

likely the reason why the CeO_2 crystallite size remains relatively constant after 15wt%Ce but the NiO size continues to decrease.

Table 5.2 Crystallite sizes and lattice parameters for NiCe catalysts.

Catalyst	NiO Crystallite Size (nm)	NiO Lattice Parameter (a)	CeO_2 Crystallite Size (nm)	CeO_2 Lattice Parameter (a)
1%NiCe	20.1	4.1807	1.2	5.4480
5%NiCe	11.5	4.1817	2.2	5.4116
10%NiCe	12.7	4.1819	3.6	5.4077
15%NiCe	13.8	4.1832	3.1	5.4097
25%NiCe	3.9	4.1867	3.0	5.4088
50%NiCe	1.8	4.1878	2.9	5.4071

The N_2 physisorption data for the NiCe catalysts shows trends for the surface area, pore volume and pore size (Table 5.3). The surface area increases as the wt% of Ce increases. The pore volumes increase between 1 and 5 and then remain constant until decreasing between 25 and 50. The pore size decreases with increasing Ce. The increasing surface area is mainly attributed to the decreasing size of the NiO crystallites. The drastic change in the pore volume and pore size in the 50wt% NiCe catalyst shows a collapse of the pore structure the catalyst. This likely means the amorphous phase is replaced by a very ordered ceria lattice doped with nickel oxide, and remaining amorphous NiO, since the lattice parameter remains small and the size of the CeO_2 crystallite remains the same. However this would be hard to confirm without further analysis such as EXAFS to determine the local structure.

Table 5.3 N_2 Physisorption data for the series of 1-50wt% NiCe catalysts.

Catalyst	BET Surface Area (m^2/g)	Pore Volume (cm^3/g)	Pore Size (Å)
1%NiCe	46.16	0.28	178.87
5%NiCe	63.97	0.38	170.02
10%NiCe	70.17	0.36	142.89
15%NiCe	87.05	0.38	133.83
25%NiCe	83.35	0.36	118.59

50%NiCe	105.96	0.16	48.1

The characterization data from this study and the characterization performed by Solsona et.al. seems to vary quite a bit. The surface areas are all very similar except for the 50wt% Ce samples but the XRD is drastically different. These differences may be due in part to the 400 °C calcination used in this study to keep materials consistent with the CeNiNb previously prepared. Their XRD data profiles look similar to the ones presented here however, for nearly every sample they claim a size of ~10 nm for both the NiO and CeO_2. Therefore, the data presented herein is likely to have a more thorough analysis. The characterization data shows that even with only the small change in temperature between the two studies, drastic changes in their physical properties can be identified. The flow reactor results also seems to be drastically different from the results of their study.

The conversion of ethane by the NiCe samples (Figure 5.4) in this study increases with increasing Ce content up to 25wt% and then decreases at 50wt%Ce. This is in agreement with their data. However, the selectivity of the catalysts in this study is much lower by 20-30 percent and decrease with increasing Ce concentrations. This shows that the catalysts that were prepared in this study are facilitating rapid uptake and transfer of oxygen to the active sites in the catalysts but that the oxygen species formed are leading to combustion products rather than the desired ethylene product. It is strange that the properties of these catalysts are so different from the ones that Solsona et.al prepared. However, it does seem to show that the increased activity of the CeNiNb is not from the Ni-Ce interaction. The 1%NiCe has the lowest activity of all of these catalysts.

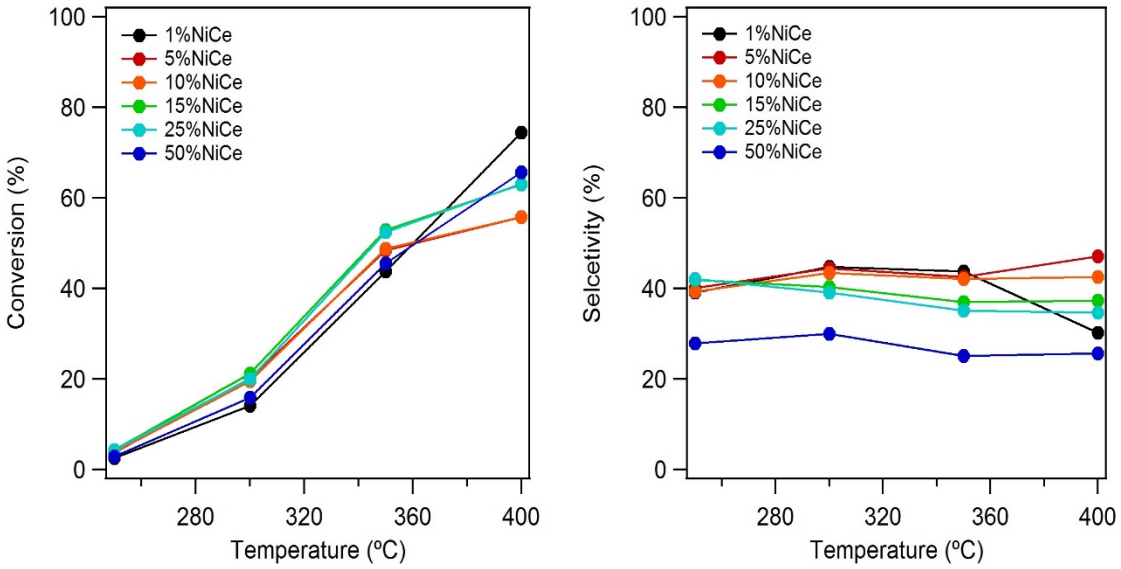

Figure 5.4 Conversion of ethane (left) and selectivity of ethylene (right) for NiCe catalysts. 1wt%NiCe(black), 5wt%NiCe(red), 10wt%NiCe(orange), 15wt%NiCe(green), 25wt%NiCe(light blue), 50wt%NiCe(dark blue).

After looking at the trends of the ceria and titania with nickel individually, new catalysts were prepared to look at the combined effects of Ce and Ti as additives to NiO. The titania has already been shown to have similar electronic properties to the Nb and it was assumed that Ce would have the same effect it had in the CeNiNb study. The results were then compared to the results obtained using the CeNiNb catalysts. The titania molar ratio was kept at a constant molar ratio of 0.25 Ti:Ni and 1, 5, 20wt% Ce was added in a preparation similar to the CeNiNb catalysts.

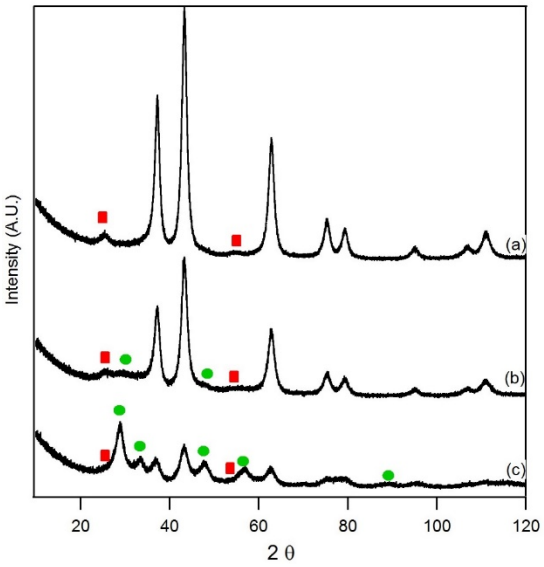

Figure 5.5 X-ray diffraction pattern for the series of NiTiCe. (a) 1wt%NiTiCe, (b) 5wt%NiTiCe, and (c) 20wt%NiTiCe. Red Squares (TiO2), Green circles (CeO2), remainder of the peaks (NiO).

The prepared NiTiCe catalysts were analyzed by powder XRD. The powder XRD data (Figure 5.5) shows that in the 1wt%NiTiCe oxide sample only the NiO and TiO_2 are observed. In the 5 and 20wt%Ce samples all three phases are present although it is very difficult to distinguish between the TiO_2 and the CeO_2 phases due to the peaks of the two phases overlapping. The crystallite size of all three phases remains fairly constant through all three samples showing that the CeO_2 likely doesn't have much of an interaction with the other two phases. The fact that there is no real change in the NiO crystallite size also suggests that the Ti stabilizes the NiO making it more difficult for CeO_2 to inhibit the aggregation as was seen in the NiCe catalysts.

After the XRD profiles were analyzed the N_2 physisorption studies were performed. The surface areas obtained from N_2 adsorption are reported in Table 5.4. All of the properties of the NiTiCe seem to be combinations of the NiTi and the NiCe already outlined. The large surface areas are more similar to the NiTi catalysts whereas the pore size and pore volumes are more

similar to the NiCe. This suggests that the TiO_2 has a strong interaction with the NiO but that the CeO_2 does not.

Table 5.4 Crystallite sizes for the NiO, TiO_2, and CeO_2 phases from powder XRD and the N_2 adsorption data for NiTiCe samples NiNb is inserted for comparison.

Cataylst	NiO Crystallite Size (nm)	TiO_2 Crystallite Size (nm)	CeO_2 Crystallite Size (nm)	BET Surface Area (m^2/g)	Pore Volume (cm^3/g)	Pore Size (Å)
NiNb	8.8	N/a	N/a	142.65	0.54	116.85
1%Ce NiTiCe	6.7	1.4	<0.5	137.18	0.56	128.91
5%Ce NiTiCe	6.4	1.8	3.4	161.31	0.61	115.84
20%Ce NiTiCe	6.8	1.4	3.2	153.21	0.33	62.06

With the characterization data finished, the reactivity of the catalysts was assessed in the flow reactor using the conditions stated in Chapter 2. The catalysts show incremental increases in the conversion from the 1-5wt%Ce and then for the 5- 20wt%Ce. The selectivity of the 1 and 5wt% samples are relatively equal, but the 20wt%Ce sample has a drastic decrease in the selectivity. It is clear from the high conversion and low selectivity of the 20%NiTiCe that most of the increased activity is mainly leading to combustion products. This may be partly due to the fact that Ti may be participating in the oxygen transfer similar to the function of Ce.[10] Based on just the conversion and selectivity data these catalysts are not as effective as the CeNiNb catalyst. However, despite the slightly lower selectivity the high conversion leads to higher ethylene yields than the CeNiNb catalysts at both 300 and 350°C.

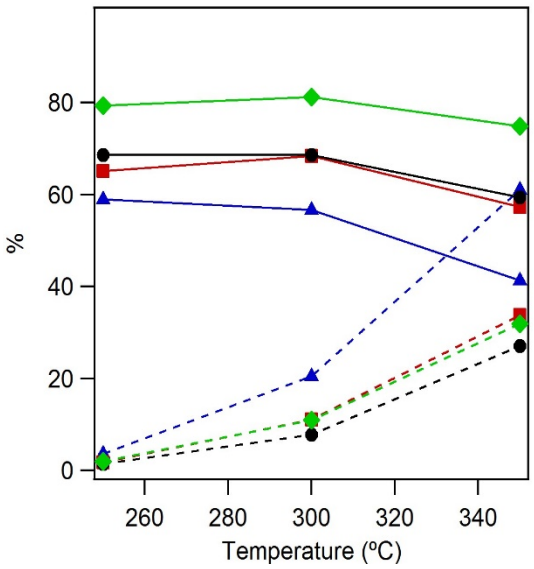

Figure 5.6 Percent conversion (dotted lines) of ethane and percent selectivity of ethylene (solid lines) for NiTiCe catalysts. Green 0.5%CeNiNb (green),1%NiTiCe (black), 5%NiTiCe (red), 20%NiTiCe (blue).

Discussion

The NiTiCe study gives some great insight into various properties of nickel-based catalysts for the ODH of ethane. First, the catalysts' overall activity is very similar to the CeNiNb catalyst. This shows that Ti is a good substitute for Nb if a cheaper alternative is needed. It also shows that the rapid uptake and transfer of oxygen by the CeO_2 is compatible with other Nb alternatives. One important difference is that unlike the CeNiNb catalyst the NiTiCe catalyst has better activity with higher Ce content whereas the CeNiNb has higher activity at low Ce content. This seems to add even further evidence to the theory that the Ce-Nb interaction leads to the Ce participating in the redox activity of the 0.25%CeNiNb catalysts since the low concentration of Ce activity is not observed in the NiTiCe catalysts.

The investigation of the effect of titania additives in the NiTi oxide catalysts shows that despite differences in the preparation method from previous reports the Ti still seems to be doping into the lattice of the NiO. It also alters the electronic properties of the NiO allowing for

higher selectivity to be observed. Excess Ti leads to amorphous character and expands the lattice. Further characterization would be necessary to validate at what concentrations amorphous character vs. doping character occur for this preparation method. Our catalysts seem to support all previous reports that multiple higher valence metal oxides can have similar electronic effects as the niobium dopant despite the type of preparation used.

The NiCe oxide catalysts that were prepared in this report were not as closely related to the ones prepared by Solsona et.al. as was desired. Their properties varied widely except for the trend in the conversion of ethane. The difference, however, was that the catalysts prepared in this study lead to combustion products. The fact that the activity is the highest only when large amounts of Ce are present for both studies indicates that the activity observed in the CeNiNb study for low wt%Ce must be correlated to the interaction of Nb. Based on the evidence from the low wt% CeNiNb study it seems more clear that the increased activity is from a Ce – O – Nb bond since this activity is not exhibited by either the NiNb or the NiCe on their own.

References

1. Zhou, Q.; Zhou, D.; Wu, Y.; Wu, T., Oxidative dehydrogenation of ethane over RE-NiO (RE=La, Nd, Sm, Gd) catalysts. *Journal of Rare Earths* **2013,** *31* (7), 669-673.
2. Zhu, H.; Dong, H.; Laveille, P.; Saih, Y.; Caps, V.; Basset, J.-M., Metal oxides modified NiO catalysts for oxidative dehydrogenation of ethane to ethylene. *Catalysis Today* **2014,** *228*, 58-64.
3. Zhu, H.; Rosenfeld, D. C.; Anjum, D. H.; Sangaru, S. S.; Saih, Y.; Ould-Chikh, S.; Basset, J.-M., Ni–Ta–O mixed oxide catalysts for the low temperature oxidative dehydrogenation of ethane to ethylene. *Journal of Catalysis* **2015,** *329*, 291-306
4. Delgado, D.; Solsona, B.; Ykrelef, A.; Rodríguez-Gómez, A.; Caballero, A.; Rodríguez-Aguado, E.; Rodríguez-Castellón, E.; López Nieto, J. M., Redox and Catalytic Properties of Promoted NiO Catalysts for the Oxidative Dehydrogenation of Ethane. *The Journal of Physical Chemistry C* **2017,** *121* (45), 25132-25142.
5. Zhu, H.; Rosenfeld, D. C.; Harb, M.; Anjum, D. H.; Hedhili, M. N.; Ould-Chikh, S.; Basset, J.-M., Ni–M–O (M = Sn, Ti, W) Catalysts Prepared by a Dry Mixing Method for Oxidative Dehydrogenation of Ethane. *ACS Catalysis* **2016,** *6* (5), 2852-2866.
6. Solsona, B.; Concepcion, P.; Hernández, S.; Demicol, B.; Nieto, J. M., *Oxidative dehydrogenation of ethane over NiO–CeO 2 mixed oxides catalysts*. 2012; Vol. 180.

7. Park, J. L.; Balijepalli, S. K.; Argyle, M. D.; Stowers, K. J., Low Temperature Oxidative Dehydrogenation of Ethane by Ce-Modified NiNb Catalysts. *Industrial & Engineering Chemistry Research* **2018,** *57* (15), 5234-5240.
8. K. Martin and G. McCarthy: North Dakota State Univ., Fargo, ND, USA, ICDD Grant-in-Aid (1991).
9. Zhu, H.; Ould-Chikh, S.; Anjum, D. H.; Sun, M.; Biausque, G.; Basset, J.-M.; Caps, V., Nb effect in the nickel oxide-catalyzed low-temperature oxidative dehydrogenation of ethane. *Journal of Catalysis* **2012,** *285* (1), 292-303.
10. Jayashree, S.; Ashokkumar, M., Switchable Intrinsic Defect Chemistry of Titania for Catalytic Applications. *Catalysts* **2018,** *8* (12), 601.

Chapter 6: Ni-Based Catalysts Supported on Silica Doped Alumina Supports for the ODH of Ethane

Introduction

The dehydrogenation of small chain alkanes continues to be a crucial process in the development of commodity chemicals.[1] Although this process has been used for decades and has seen incremental improvements over the years, the high temperatures are costly in terms of energy and environmental impact. In recent years however, oxidative dehydrogenation reactions have been shown to be a suitable alternative to direct dehydrogenation.[2,3] This process significantly decreases the reaction temperature by utilizing oxygen as a co-feed with the alkane.

The oxidative dehydrogenation of ethane to form ethylene has been studied extensively and nickel based catalysts are promising candidates for commercialization if higher conversions can be achieved. [4-7] One way to facilitate this is to use an inert oxide support,[8] which increases reaction sites and decreases the catalyst cost. Alumina is commonly used as a support in catalysis due to its large surface area and acidic properties. Multiple groups have shown extremely good selectivities with moderate yields using nickel supported catalysts for ODH.[9-12]

In more recent studies, the structure of the NiO or the electronic properties of the lattice have been altered in order to improve the activity and selectivity of the catalyst. In one study Capek et.al. showed[13] that by using an organic nickel precursor ($Ni(acac_2)_2$) rather than an inorganic nickel precursor ($Ni(NO_3)_2$) they could form small NiO crystals that led to higher activity. However when using $Ni(NO_3)_3$ a tetrahedral Ni species was formed that led to higher selectivity but lower activity. Later Kout et.al. showed[14] that the calcination temperature of the catalyst also shows a profound effect on the type of nickel species present. At high calcination temperatures large amounts of $NiAl_2O_4$ spinel species formed. The presence of this species

gradually increases the selectivity but decreases the activity. Once the concentration of $NiAl_2O_4$ passes a certain amount the reaction is no longer active.

In another study by Lemonidou et.al. nickel salts were co-precipitated with alumina alkoxides in the ratio of 1 to 50 Ni:Al. This study showed[11] that as the Ni-Al ratio increased up to the ratio of 30:1 Ni:Al the selectivity of the catalyst increases. The selectivity of these catalysts was attributed to the alumina doping into the cationic vacancies of the NiO lattice. This reduces the available electrophilic oxygen species that lead to combustion. Later in the study the catalyst was further optimized by substituting an organic nickel precursor for the inorganic precursor as shown by Capek et. al. and further increased the selectivity by approximately 20%.

In all of the previous studies for the oxidative dehydrogenation of ethane over NiO/Alumina catalysts it is clear that a strong interaction between the nickel and alumina is required to optimize the ethylene output. However, one thing that has not specifically been discussed in these papers is how the acidity of the support influences the binding of the active phase and if changing the acidity of the support will lead to higher selectivities or better activity of the catalyst. In this study a novel silica doped alumina that has tunable acidic properties is used to investigate the role of the acid properties of the support for binding of the NiO. Ultimately the support interactions and geometries will be used to determine how optimization of the catalyst towards ethylene production is affected.

Procedures for Catalyst Preparation

Preparation γ-Alumina support[15]: A 100 g batch of γ-Alumina support material was prepared by mixing 400g of aluminum isopropoxide (AIP) with 176mL of DI water in a large mixer for 20 minutes. This creates a paste which is calcined in an oven with a ramp of 5°C/min to 700°C and the held at that temperature for 2 hour before returning to room temperature.

Preparation Silica doped alumina (SDA) support[16]: A 100 g batch of silica doped alumina support material was prepared by mixing 380.61g of aluminum isopropoxide, (AIP) with 173mL of DI water, and 18.4mL of tetraethylorthosilicate (TEOS) in a large mixer for 20 minutes. This creates a paste which is calcined in an oven with a ramp of 5°C/min to any temperature from 700-1100°C and the held at that temperature for 2 hour before returning to room temperature.

Once the supports are prepared the pore volume of the supports must be analyzed by N_2 adsorption studies (which will be outlined later). With a known pore volume for each support a solution of the active species can be prepared. The goal is to make the concentration of the solution such that when you add only the pore volume/g support you get the desired % active species by weight. This is typically referred to as weight percent active species or (wt%). In some cases large wt% leads to precipitation out of solution so multiple impregnations are necessary.

Preparation 2.3 Incipient wetness impregnation of nickel on γ-Alumina: 3.87 mL of a 0.9025 M solution of Nickel nitrate was added dropwise to 2.76g of γ-Alumina support. The two were mixed together with a spatula for ten minutes allowing the solution to wick into the entirety of the pore structure. The catalyst is then dried overnight at 100°C and then calcined in an oven at a ramp rate of 3°C/min to 400°C and then held at that temperature for 4 hours. This gets us to 8wt% NiO on the support. This entire process must be repeated a second time to reach 16wt% NiO on the support.

Preparation incipient wetness impregnation of 16wt% nickel on 5%SDA calcined at 700°C: 4.29 mL of a 0.814M solution of nickel nitrate was added dropwise to 2.76g of 5%SDA700 support. The two were mixed together with a spatula for ten minutes allowing the

solution to wick into the entirety of the pore structure. The catalyst is then dried overnight at 100°C and then calcined in an oven at a ramp rate of 3°C/min to 400°C and then held at that temperature for 4 hours. This gets us to 8wt% NiO on the support. This entire process must be repeated a second time to reach 16wt% NiO on the support.

Preparation Incipient wetness impregnation of 16wt% nickel on 5%SDA calcined at 1100°C: 4.23 mL of a 0.946M solution of nickel nitrate was added dropwise to 2.76g of 5%SDA1100 support. The two were mixed together with a spatula for ten minutes allowing the solution to wick into the entirety of the pore structure. The catalyst is then dried overnight at 100°C and then calcined in an oven at a ramp rate of 3°C/min to 400°C and then held at that temperature for 4 hours. This gets us to 8wt% NiO on the support. This entire process must be repeated a second time to reach 16wt% NiO on the support.

Data

The first step in analyzing these supported nickel catalysts is the characterization of the catalysts. Powder X-Ray diffraction was performed, as discussed in Chapter 2, on all the catalysts prepared by incipient wetness impregnation. The figures for the diffraction patterns are organized by support below. All the data for the Al_2O_3 catalysts (Figure 6.1), all the data for the 5%SDA700 catalysts (Figure 6.2), all the data on the 5%SDA1100 catalysts (Figure 6.3) are grouped for comparison. There is not much difference between the support itself and the 8wt%, 16wt%, and 16wt% calcined at 500°C for the Al_2O_3 catalysts. The NiO from the commercial source is used as a reference on where the NiO peaks are expected and is set in each diffraction pattern. The NiO peaks were not observed. The fact that they are not observed indicates that the NiO crystallites are well distributed and that the calcination temperature of 400-500°C does not allow for significant aggregation of particles. A similar trend is seen in the samples prepared on

the 5%SDA700 support. In all the diffraction patterns for the 8wt%, 16wt%, and 16wt% NiO calcined at 500°C on 5%SDA700 no peak representing NiO were observed.

In the diffraction patterns for the 5%SDA1100 supported samples, the gamma phase of the alumina is more defined and a few of the peaks representing the NiO phase were observed. The most apparent peak is the one at 43° 2θ. This represents the (200) plane of cubic NiO.[20] Other characteristic peaks for NiO are barely observable in the 16wt%, and 16wt% calcined at 500°C. The three observed peaks allowed for the calculation of the crystallite size of NiO using the Scherrer equation. The sizes were 4.2 and 4.8 nm respectively. This shows that by using these mesoporous alumina supports we can obtain high dispersions of the active phase enabling the maximum number of active sites for the reaction.

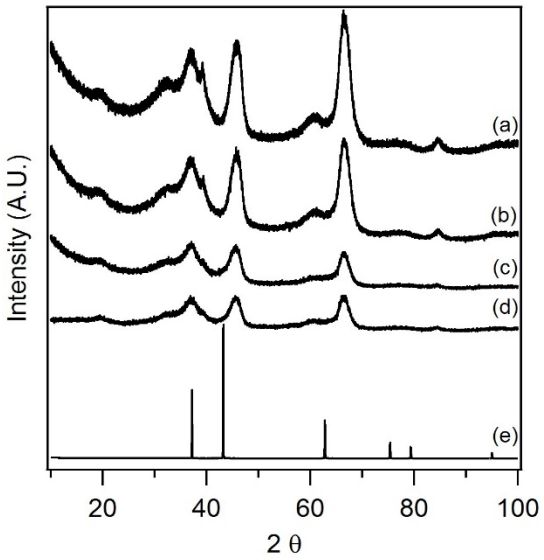

Figure 6.1 Powder XRD for the series of gamma alumina catalysts. (a) Al_2O_3 support, (b) 8% NiO/Al_2O_3, (c) 16% NiO/ Al_2O_3, (d) 16%NiO/ Al_2O_3 calcined at 500°C, (e) commercial NiO control.

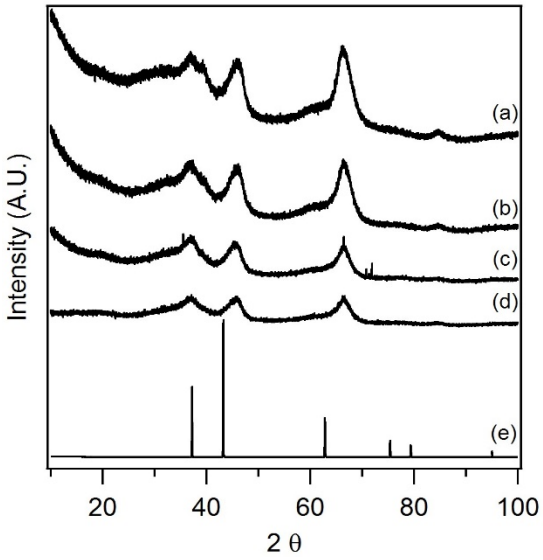

Figure 6.2 Powder XRD for the series of 5%SDA700 catalysts. (a) 5%SDA700 support, (b) 8% NiO/5%SDA700, (c) 16% NiO/5%SDA700, (d) 16%NiO/5%SDA700 calcined at 500°C, (e) commercial NiO control.

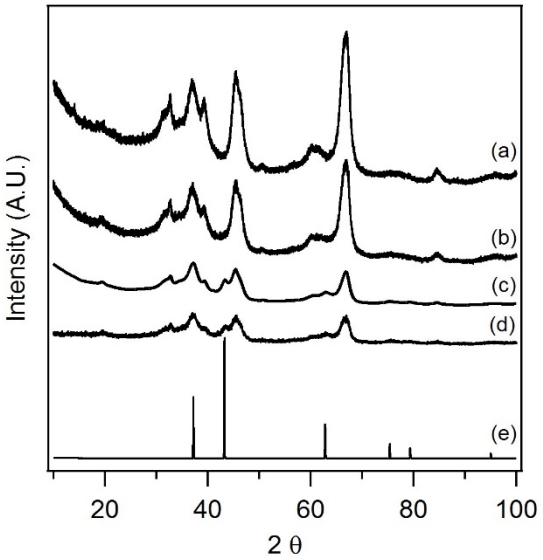

Figure 6.3 Powder XRD for the series of 5%SDA1100 catalysts. (a) 5%SDA1100 support, (b) 8% NiO/5%SDA1100, (c) 16% NiO/5%SDA1100, (d) 16%NiO/5%SDA1100 calcined at 500°C, (e) commercial NiO control.

One of the advantages of these silica doped aluminas is the fact that the doping of the silica allows the gamma phase of alumina to be stabilized at high temperatures.[21] N_2 adsorption studies were performed in order to get a better understanding of the physical properties of the

supports and how the support properties change with the addition of NiO. Nitrogen adsorption studies were conducted (Table 6.1). Due to the unique stability of the support the surface area and pore volume for the 5%SDA1100 is still relatively large. This is in contrast to the other non-doped alumina where calcination temperatures above 1000°C start to form alpha phase alumina[22] which has a much lower surface area.

Table 6.1 Physical properties of alumina supported catalysts.

Catalyst	Surface area (m^2/g)	Pore Volume (cm^3/g)	Pore diameter (nm)	NiO crystallite size (nm)
SDA700	337.1	1.400	16.6	
Al_2O_3	233.5	1.371	23.5	
SDA1100	182	1.195	26.5	
8% NiO/SDA700	273.1	0.468	12.1	no
16% NiO/SDA700	277	0.411	21.6	no
16% NiO/SDA700 500°C	220.0	0.385	16.2	no
8% NiO/Al_2O_3	228.5	0.742	13.6	no
16% NiO/Al_2O_3	205.7	0.623	16.1	no
16% NiO/Al_2O_3 500°C	182.3	0.600	11.8	no
8% NiO/SDA1100	182	1.040	19.2	no
16% NiO/SDA1100	165.4	0.878	15.7	4.2
16% NiO/SDA1100 500°C	168.9	0.957	15.2	4.8

The NiO on Al_2O_3, and the NiO on SDA1100 surface areas do not vary drastically from the value of the original support (Table 6.1). This suggests very high dispersion of the NiO phase, it also shows that higher wt% NiO can be added to these supports to further maximize their activity. The large initial drop in surface area in the SDA700 catalysts is likely the result of the NiO plugging a large majority of the micropores[23] of the support. After this initial drop the surface area does not change significantly suggesting that once the micropores have been plugged the NiO phase also distributes quite well through the rest of the pores in this support. One other thing to consider is the changes observed in the pore volumes of each sample. The

large changes in the pore volume of the SDA700, and the Al_2O_3 samples suggest that most of the NiO resides in the pores of the support. However, with the NiO added to the SDA1100 it is more likely that it ended up on the surface of the support since the pore volume remains relatively constant. With more NiO on the surface, this also explains why the NiO peak is only observed on the SDA1100.

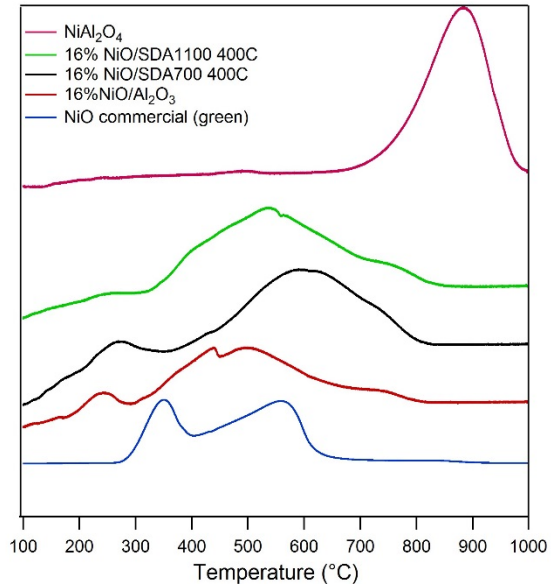

Figure 6.4 H2-TPR of data for the 16wt% NiO samples from 100-1000ºC at 10ºC/min. NiAl2O4 (pink), 16%NiO/SDA1100 (green), 16%NiO/SDA700 (black), 16%NiO/Al_2O_3 (red), NiO Sigma-aldrich (blue).

The reducibility of the NiO species on the catalysts was investigated using H_2-TPR analysis. In Figure 6.4 it shows in blue the reduction profile of a pure NiO (99.8%) from a commercial source. The red, black and green profiles are those of 16% NiO/Al_2O_3, 16%NiO/SDA700, and 16%NiO/SDA1100 respectively. The pink profile is a sample of 16%NiO/Al_2O_3 calcined at 1000ºC representing the reduction of $NiAl_2O_4$ spinel species. The first peak in all the sample profiles around 270ºC is likely the reduction of Ni_2O_3 or surface Ni-O species that formed from weakly bound nickel oxide sites.[24] The second peak which varies drastically between all the samples is the reduction of the Ni-O bond of the lattice oxygen. The

variance in the reduction of this second peak shows that the Ni-O bond for the 16%NiO/SDA700 is the hardest to reduce and predicts that it will have the lowest activity of the catalysts. There is also a third peak in all three samples at approximately 750ºC. This peak represents the formation and reduction of a $NiAl_2O_4$ phase.

The reason for the difference in where the NiO is observed for these supports is likely due to the acidity of these supports. Based on previous reports, the SDA700 and the Al_2O_3 have higher acidity and thus better binding sites throughout the material. The SDA1100 has almost no acid sites and as a result the impregnated material is likely wicked to the surface as the catalysts dries. This will be confirmed later using acid site analysis.

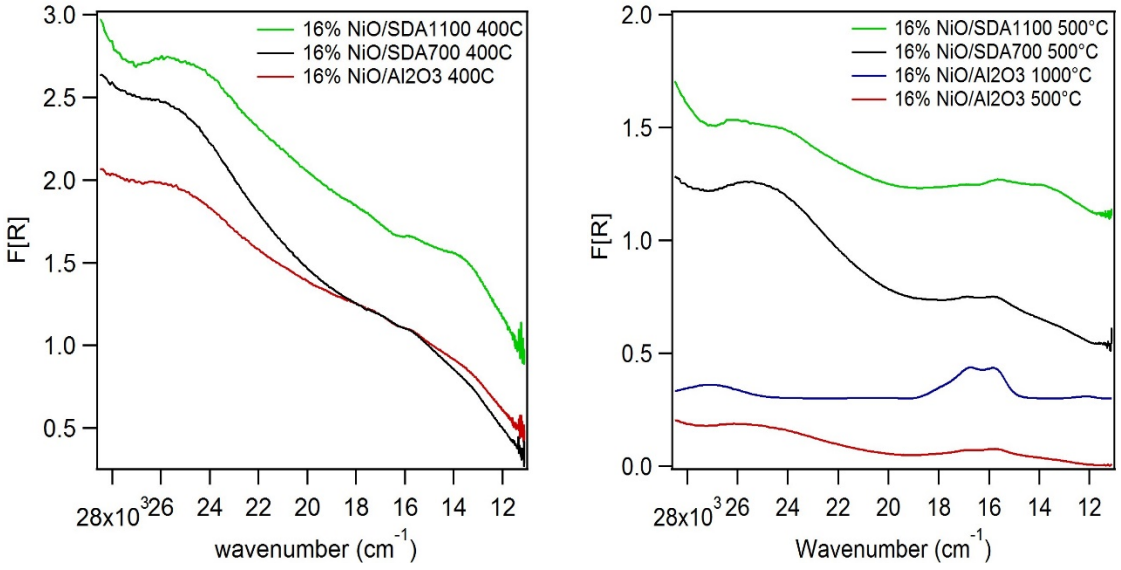

Figure 6.5 UV-Vis spectrum of 16wt% NiO catalysts calcined at 400, 500°C. NiO/SDA1100 (green), NiO/SDA700 (red), NiO/Al_2O_3 (red). NiO/ Al_2O_3 calcined at 1000°C (Blue).

It has been reported that the formation of a tetrahedral NiO species or a $NiAl_2O_4$ spinel phase had an influence on the selectivity towards ethylene in the ODH reaction.[25] This phase is not observable by XRD and is somewhat hinted at in the reduction profiles. However, to confirm the structure UV-Vis spectra were taken (Figure 6.5). According to Smolákov et.al. the doublet

at 15,770 and 16,690 cm^{-1} represents the formation of the octahedral Ni or the $NiAl_2O_4$ spinel phase. In both the 16%NiO/5%SDA700 and the 16%NiO/5%SDA1100 a very small broad doublet is observed in the spectra. However, the 16%NiO/Al_2O_3 does not exhibit these peaks. When the catalysts are calcined at the higher temperature of 500°C in order to better observe the $NiAl_2O_4$, the peaks are more defined. The presence of this phase is the most concentrated in the following order for the samples: 16%NiO/5%SDA700 > 16%NiO/5%SDA1100 > 16%NiO/Al_2O_3. The formation of this phase correlates to an increased selectivity up to a certain point at which the $NiAl_2O_4$ phase diminishes the activity of the catalyst.

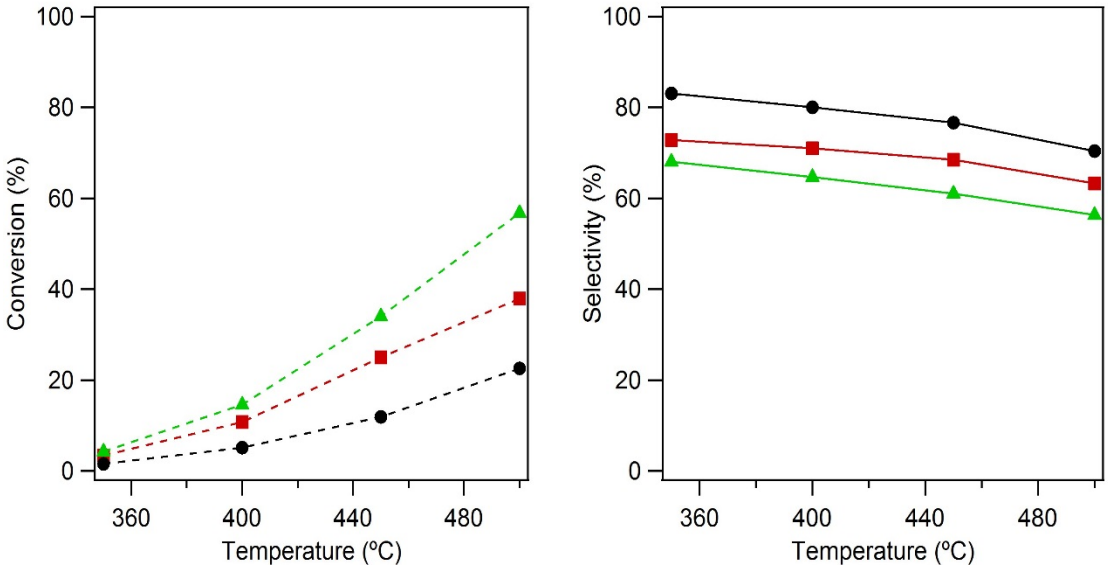

Figure 6.6 Conversion (left) and selectivity (right) vs. temperature from 350-500ºC for 16wt% NiO/Al_2O_3 (red), 16wt% NiO/SDA700 (black), and 16wt% NiO/SDA1100 (green) samples.

The conversion and selectivity data for the conversion of ethane to ethylene at a total flow rate of 10mL/min and 100mg of catalyst is shown for 16%NiO/Al_2O_3, 16%NiO/SDA700, and 16% NiO/SDA1100 (Figure 6.6). Both the conversion (dotted lines) and selectivity (solid lines) are represented for the 16%NiO/SDA700 (black), the 16%NiO/Al_2O_3 (red) and the 16%NiO/SDA1100 (green). The selectivity of these catalysts are moderately high which is

indicative of the alumina binding very strongly with the SDA700, less with the Al_2O_3 and the least with SDA1100. This agrees with the UV-Vis data already shown.

The conversion and selectivity of these catalysts are somewhat inversely proportional to each other, or in other words, the one with the highest selectivity has the lowest activity and the one with the highest activity has the lowest selectivity. This is similar to the reports of other nickel on alumina catalysts. The reason for this has to do with the NiO activation mechanism for ethane ODH. The higher activity is related to higher amounts of electrophilic oxygen species available, which also leads to overoxidation products. Whereas the selectivity is associated with more tightly bound and less electrophilic oxygens that lead to low ethylene production but with high selectivity.[4]

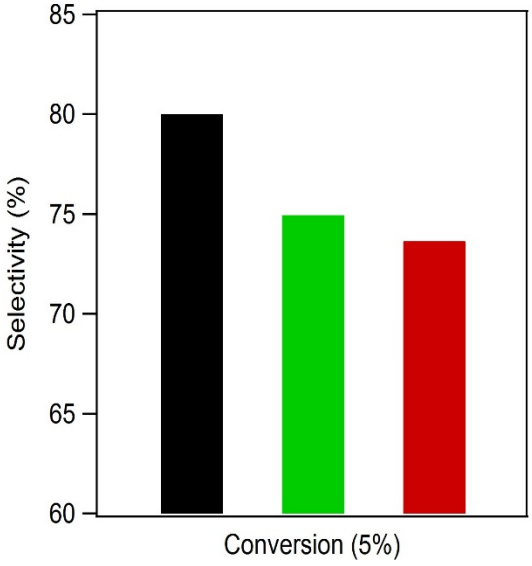

Figure 6.7 The selectivity of 16wt% NiO catalysts at 5% conversion. 16%NiO/SDA700(black), 16% NiO/SDA1100 (green), and 16%NiO/Al_2O_3 (red).

In order to get an independent comparison of the selectivity of these catalysts, the selectivities were assessed at a constant conversion of 5% at 400°C by varying the flow rates from (10-50mL/min). The 16%NiO/SDA700 and has the highest selectivity. The order of the

selectivity for the 16%NiOSDA1100 and the 16%NiO/Al_2O_3 change when compared at similar conversion the 16%NiOSDA1100 and has a slightly higher selectivity than the 16%NiO/Al_2O_3. Since the selectivity for these types of catalysts has been attributed to the formation of the $NiAl_2O_4$ phase this suggests that there is a larger concentration of this phase in this sample. It also suggests that the addition of the silica in the preparation of these samples helps form this phase.

The selectivity and conversion data presented show a convincing argument that the 16wt% NiO/SDA700 might be the best catalyst if used at high temperature. However, from the rate data it is clear that the 16wt%NiO/SDA1100 produces the highest amount of ethylene at every temperature measured. This suggests that the conversion and selectivity should never be independently reported from the rate data for ODH catalysts.

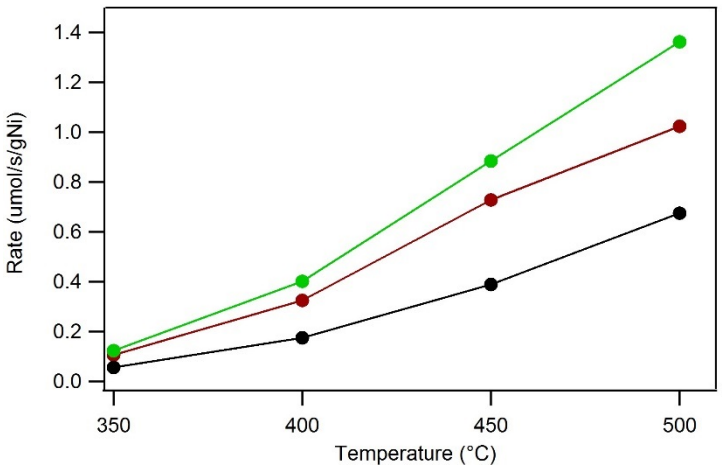

Figure 6.8 Rate of ethylene per g Ni for 16wt% NiO/SDA1100 (green), 16wt% NiO/Al_2O_3 (red), and 16wt% NiO/SDA700 (black).

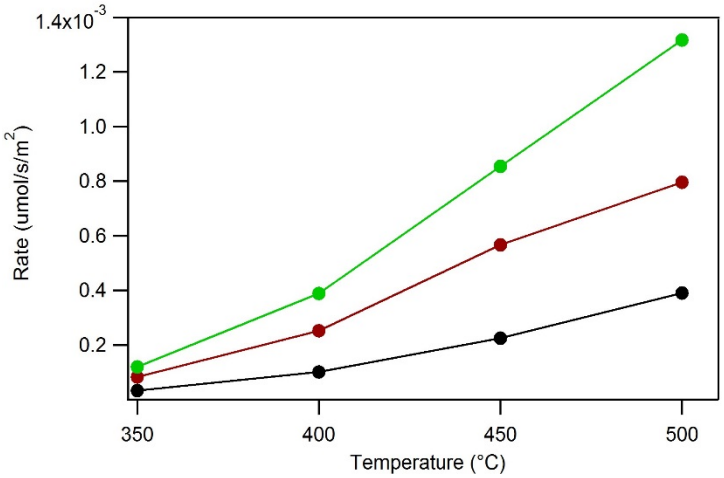

Figure 6.9 Rate of ethylene per surface area for 16wt% NiO/SDA1100 (green), 16wt% NiO/Al_2O_3 (red), and 16wt% NiO/SDA700 (black).

The rates for these catalysts were calculated using the umol of ethylene per gram nickel (Figure 6.8) and the umol of ethylene per surface area of the catalyst (Figure 6.9). In both cases the 16%NiO/SDA1100 (green) produces the highest amount of ethylene with the second highest being 16%NiO/Al_2O_3 (red) and 16%NiO/SDA700 (black) being the least productive. In all cases the rate of ethylene/gNiO doubles when the catalyst loading was increased from 8wt% NiO (not shown) to 16wt%NiO.

Discussion

In this study we have shown the preparation and catalytic activity of nickel catalysts supported on silica doped alumina towards the ODH of ethane. These catalysts show a higher concentration of $NiAl_2O_4$ which leads to high selectivity at the cost of catalyst activity. The very high dispersion of the active phase leads to high activities. This suggests that even at 16wt% NiO we haven't saturated our support and as a result could continue to increase the loadings to maximize our ethylene yields. These initial studies show that with further optimization these catalysts could be very efficient catalysts for ODH reactions.

It was suggested in one of the previous reports for nickel on alumina that the surface area has an impact on the overall activity.[9] This does not appear to be the case for our samples. The samples in our study all seem to have activities that are independent of surface area. This is shown by the fact that the 16%NiO/SDA1100 has the smallest surface area but exhibits the highest rate. This is opposite of what was observed with previous reports.

In order to make specific conclusions regarding the role of the acidity on the catalyst, the ammonia TPD for total acid sites and the pyridine FTIR will be completed in the near future. One major reason for this is the selectivities at 5% conversion seem to suggest that either the SDA1100 has adopted more acid sites leading to better binding and more $NiAl_2O_4$ formation or that it is simply a direct effect of the Si stabilizing the structure allowing for easy formation of the nickel spinel phase. In the previous report on the preparation of these materials the ammonia TPD shows that the SDA700 has the highest amount of acid sites, the Al_2O_3 having the next highest and the SDA1100 having very few. If this were true the selectivity of ethylene would follow the same trend. We have yet to confirm that the addition of the NiO does not drastically change the amount of acidity.

References

1. Bender, M., An Overview of Industrial Processes for the Production of Olefins – C4 Hydrocarbons. *ChemBioEng Reviews* **2014,** *1* (4), 136-147.
2. Thorsteinson, E. M.; Wilson, T. P.; Young, F. G.; Kasai, P. H., The oxidative dehydrogenation of ethane over catalysts containing mixed oxides of molybdenum and vanadium. *Journal of Catalysis* **1978,** *52* (1), 116-132.
3. Gärtner, C. A.; van Veen, A. C.; Lercher, J. A., Oxidative Dehydrogenation of Ethane: Common Principles and Mechanistic Aspects. *ChemCatChem* **2013,** *5* (11), 3196-3217.
4. Heracleous, E.; Lemonidou, A., Ni–Nb–O mixed oxides as highly active and selective catalysts for ethene production via ethane oxidative dehydrogenation. Part I: Characterization and catalytic performance. *Journal of Catalysis* **2006,** *237* (1), 162-174.
5. Zhu, H.; Ould-Chikh, S.; Anjum, D. H.; Sun, M.; Biausque, G.; Basset, J.-M.; Caps, V., Nb effect in the nickel oxide-catalyzed low-temperature oxidative dehydrogenation of ethane. *Journal of Catalysis* **2012,** *285* (1), 292-303.

6. Zhu, H.; Rosenfeld, D. C.; Anjum, D. H.; Caps, V.; Basset, J.-M., Green Synthesis of Ni–Nb oxide Catalysts for Low-Temperature Oxidative Dehydrogenation of Ethane. *ChemSusChem* **2015,** *8* (7), 1254-1263.
7. Védrine, J. C., Heterogeneous Partial (amm)Oxidation and Oxidative Dehydrogenation Catalysis on Mixed Metal Oxides. *Catalysts* **2016,** *6* (2), 22.
8. Zhang, X.; Gong, Y.; Yu, G.; Xie, Y., Oxygen species on NiO/Al2O3 and their reactivities. *Journal of Molecular Catalysis A: Chemical* **2002,** *180* (1), 293-298.
9. Zhang, X.; Liu, J.; Jing, Y.; Xie, Y., Support effects on the catalytic behavior of NiO/Al2O3 for oxidative dehydrogenation of ethane to ethylene. *Applied Catalysis A: General* **2003,** *240* (1), 143-150.
10. Heracleous, E.; Lee, A.; Wilson, K.; Lemonidou, A., Investigation of Ni-based alumina-supported catalysts for the oxidative dehydrogenation of ethane to ethylene: structural characterization and reactivity studies. *Journal of Catalysis* **2005,** *231* (1), 159-171.
11. Skoufa, Z.; Xantri, G.; Heracleous, E.; Lemonidou, A. A., A study of Ni–Al–O mixed oxides as catalysts for the oxidative conversion of ethane to ethylene. *Applied Catalysis A: General* **2014,** *471*, 107-117.
12. Garbarino, G.; Riani, P.; Infantes-Molina, A.; Rodríguez-Castellón, E.; Busca, G., On the detectability limits of nickel species on NiO/γ-Al2O3 catalytic materials. *Applied Catalysis A: General* **2016,** *525*, 180-189.
13. Smoláková, L.; Botková, Š.; Čapek, L.; Priecel, P.; Sołtysek, A.; Kout, M.; Matějová, L., Precursors of active Ni species in Ni/Al2O3 catalysts for oxidative dehydrogenation of ethane. *Chinese Journal of Catalysis* **2013,** *34* (10), 1905-1913.
14. Smoláková, L.; Kout, M.; Koudelková, E.; Čapek, L., Effect of Calcination Temperature on the Structure and Catalytic Performance of the Ni/Al2O3 and Ni–Ce/Al2O3 Catalysts in Oxidative Dehydrogenation of Ethane. *Industrial & Engineering Chemistry Research* **2015,** *54* (51), 12730-12740.
15. Mardkhe, M. K.; Keyvanloo, K.; Bartholomew, C. H.; Hecker, W. C.; Alam, T. M.; Woodfield, B. F., Acid site properties of thermally stable, silica-doped alumina as a function of silica/alumina ratio and calcination temperature. *Applied Catalysis A: General* **2014,** *482*, 16-23.
16. Mardkhe, M. K.; Keyvanloo, K.; Bartholomew, C. H.; Hecker, W. C.; Alam, T. M.; Woodfield, B. F., Acid site properties of thermally stable, silica-doped alumina as a function of silica/alumina ratio and calcination temperature. *Applied Catalysis A: General* **2014,** *482*, 16-23.
17. Huang, B.; Bartholomew, C. H.; Woodfield, B. F., Improved calculations of pore size distribution for relatively large, irregular slit-shaped mesopore structure. *Microporous and Mesoporous Materials* **2014,** *184*, 112-121.
18. Patterson, A. L., The Scherrer Formula for X-Ray Particle Size Determination. *Physical Review* **1939,** *56* (10), 978-982.
19. Kokhanovsky, A. A., Physical interpretation and accuracy of the Kubelka–Munk theory. *Journal of Physics D: Applied Physics* **2007,** *40* (7), 2210-2216.
20. K. Martin and G. McCarthy: North Dakota State Univ., Fargo, ND, USA, ICDD Grant-in-Aid (1991).
21. Mardkhe, M. K.; Huang, B.; Bartholomew, C. H.; Alam, T. M.; Woodfield, B. F., Synthesis and characterization of silica doped alumina catalyst support with superior

thermal stability and unique pore properties. *Journal of Porous Materials* **2016,** *23* (2), 475-487
22. Lamouri, S.; Hamidouche, M.; Bouaouadja, N.; Belhouchet, H.; Garnier, V.; Fantozzi, G.; Trelkat, J. F., Control of the γ-alumina to α-alumina phase transformation for an optimized alumina densification. *Boletín de la Sociedad Española de Cerámica y Vidrio* **2017,** *56* (2), 47-54.
23. Regalbuto, J., Catalysts Preparation Science and Engineering; CRC Press: Boca Raton, FL, 2007, pp 375-400.
24. Zeng, Y.; Ma, H.; Zhang, H.; Ying, W.; Fang, D., Highly efficient NiAl2O4-free Ni/γ-Al2O3 catalysts prepared by solution combustion method for CO methanation. *Fuel* **2014,** *137*, 155-163
25. Smoláková, L.; Kout, M.; Koudelková, E.; Čapek, L., Effect of Calcination Temperature on the Structure and Catalytic Performance of the Ni/Al2O3 and Ni–Ce/Al2O3 Catalysts in Oxidative Dehydrogenation of Ethane. *Industrial & Engineering Chemistry Research* **2015,** *54* (51), 12730-12740.

Chapter 7: Summary and Conclusions

In this manuscript, the fundamental principles related to the preparation, characterization, and performance of bulk and supported nickel catalysts for ethane ODH were outlined and described. The advances demonstrated herein, are just small steps in the path towards effective commercialization of the ODH process using nickel catalysts as a means to increase efficiency in energy and cost. The first study of CeNiNb bulk catalysts pushes the boundaries of ethane ODH by almost doubling the low temperature production of ethylene.[1] Ceria nanoparticles as an additive to the nickel catalysts, observed in this mixed metal oxide solid solution, increase the rapid uptake of oxygen from the feed gas and efficiently transfer adsorbed oxygen to active NiO redox sites. This function is most prevalent at low concentrations of CeO_2. The low concentrations lead to the optimization of activity without large decreases in selectivity.

In the follow up study of the low wt% CeNiNb catalyst, the investigation provides insight into the structure of the three metal oxides and the interactions observed to then postulate the mechanism through which the high activity was obtained. All evidence seems to suggest that the key to catalyst design is the interaction between the Ce and Nb. The data indicates this interaction allows for a secondary redox site to participate in the ODH reaction. This means that the Nb not only facilitates the reduction of nonstoichiometric oxygen in the nickel,[2] as was previously hypothesized, but it also likely does the same for the ceria. This means that as Ce rapidly adsorbs oxygen from the feed it can transfer it to two different sites. The improvement of catalytic activity will be directly correlated to how many Ce – O – Nb sites are present.

The NiTiCe study confirms some of the discrepancies left open-ended in the EXAFS data from CeNiNb study and adds to the theory of the Ce-Nb interaction. In the first part of the study the NiTi series confirms that the electronic changes induced on NiO by the addition of Nb is not

unique to Nb. Any higher valence metal oxide should induce a reduction of the amount of non-stoichiometric oxygen species present by doping into the lattice at the cationic vacancy sites.[3] The higher valence species binds more strongly with the oxygen and reduces the Ni^{3+} to Ni^{2+}. The second part of the study with the series of NiCe catalysts confirms that the increased amount of ceria should increase the activity. It shows that the high activity of the CeNiNb catalysts is unique to that system giving evidence for the Ce-Nb interaction.

The third part of this study with the NiTiCe shows that Ce could have an impact on any of the combinations of Ni and a higher valent species. It also shows that if the higher valent species also has oxygen transfer properties it may lead to high activities. The improved activity observed at increasing amounts of Ce contributes to the idea that the CeNiNb catalyst is unique and that the performance at low Ce content is likely due to the Ce-Nb interaction.

The nickel supported on mesoporous aluminas is the first step in applying what was gathered from the investigations of the bulk materials. The rates of 0.2 kg ethylene/kg_{cat}/hr are a good indication that the 1 kg ethylene/kg_{cat}/hr cited as the ideal rate for commercialization[5] should be obtainable. The relationship between the support and the active species in catalysis is crucial for commercial performance. The fact that alumina can have a strong interaction with the nickel facilitating improved selectivity may rule out the necessity for adding Nb or another higher valent metal oxide. If the acidity of the support does play a role in facilitating this strong interaction, then the tunable nature of the acid sites of this support becomes a key factor in the optimization of these catalysts for commercial use.

The small advances shown in this manuscript provide valuable insight into using nickel-based catalysts for ODH reactions in general. Even though we have not quite reached the ideal rate for commercialization, we have shown that even small changes can drastically improve

those rates. This gives hope that with further analysis and increased optimization nickel catalyst will be used for ODH of alkanes in the future.

Having set some ground work for new ODH catalysts, it is important to consider some of the new directions that are now available for study. The first and easiest direction relates to why ethane was chosen in the first place. The activation of the C-H bond in ethane requires a lot of energy, which is why direct dehydrogenation occurs at 700-900C. As hydrocarbon length increases the C-H activation decreases. The fact that all the catalysts made in this study can activate ethane means that theoretically they will all work for propane, butane, pentane etc. As such it would be fascinating to see the reactivity of these different feedstocks with the 0.25CeNiNb catalyst.

Another obvious direction is to continue the optimization of the NiO on the alumina supports, especially as stated above if the acidity of the support is identified as crucial to the selectivity. Changing the silica content[6] and calcination temperature can alter the acidity of the support. On top of just the acidity studies with these supports there is also improvement through the addition of Ce that should drastically impact the activity of the overall catalyst.

A third exciting direction to follow up on would be this idea around the Ce-Nb interaction. The first part of this would be that if our theory is correct and the interaction of the Ce – O – Nb forms a new redox site active for ODH. Then it's obvious that a study should be done to prepare the Ce-Nb oxide in a way that maximizes this interaction. The second part of this idea is that the EXAFS data in the R-space indicates the bond of the Ni – O and the altered Ce – O are approximately the same distance. This suggests that one could essentially design catalysts for this reaction by creating catalysts that have redox activity but also have an optimal bond length that is desirable for ODH.

All of the above postulated directions could lead to new ODH catalysts and ultimately new options for refineries to make precursors for plastics. This would not only have an impact on productivity of olefins but also on the environment. If ODH reactions can be facilitated with reasonable yields then companies would make an easy financial choice to switch from direct dehydrogenation to ODH processes. This would lead to drastic changes in energy costs and less CO_2 emitted from lower energy usage.

References

1. Park, J. L.; Balijepalli, S. K.; Argyle, M. D.; Stowers, K. J., Low Temperature Oxidative Dehydrogenation of Ethane by Ce-Modified NiNb Catalysts. *Industrial & Engineering Chemistry Research* **2018,** *57* (15), 5234-5240.
2. Heracleous, E.; Lemonidou, A., Ni–Nb–O mixed oxides as highly active and selective catalysts for ethene production via ethane oxidative dehydrogenation. Part I: Characterization and catalytic performance. *Journal of Catalysis* **2006,** *237* (1), 162-174.
3. Heracleous, E.; Lemonidou, A. A., Ni–Me–O mixed metal oxides for the effective oxidative dehydrogenation of ethane to ethylene – Effect of promoting metal Me. *Journal of Catalysis* **2010,** *270* (1), 67-75.
4. Solsona, B.; Concepcion, P.; Hernández, S.; Demicol, B.; Nieto, J. M., *Oxidative dehydrogenation of ethane over NiO–CeO 2 mixed oxides catalysts*. 2012; Vol. 180.
5. Yun, Y. S.; Lee, M.; Sung, J.; Yun, D.; Kim, T. Y.; Park, H.; Lee, K. R.; Song, C. K.; Kim, Y.; Lee, J.; Seo, Y.-J.; Song, I. K.; Yi, J., Promoting effect of cerium on MoVTeNb mixed oxide catalyst for oxidative dehydrogenation of ethane to ethylene. *Applied Catalysis B: Environmental* **2018,** *237*, 554-562.
6. Mardkhe, M. K.; Huang, B.; Bartholomew, C. H.; Alam, T. M.; Woodfield, B. F., Synthesis and characterization of silica doped alumina catalyst support with superior thermal stability and unique pore properties. *Journal of Porous Materials* **2016,** *23* (2), 475-487.